Topical Review

Molecular adsorption on graphene

Lingmei Kong[1]**, Axel Enders**[1]**, Talat S Rahman**[2] **and Peter A Dowben**[1]

[1] Department of Physics and Astronomy, Nebraska Center for Materials and Nanoscience, Theodore Jorgensen Hall, 855 North 16th Street, University of Nebraska, PO Box 880299, Lincoln, NE 68588-0299, USA

[2] Department of Physics, University of Central Florida, 4000 Central Florida Blvd., Orlando, FL 32816, USA

E-mail: axel@unl.edu

Abstract
Current studies addressing the engineering of charge carrier concentration and the electronic band gap in epitaxial graphene using molecular adsorbates are reviewed. The focus here is on interactions between the graphene surface and the adsorbed molecules, including small gas molecules (H_2O, H_2, O_2, CO, NO_2, NO, and NH_3), aromatic, and non-aromatic molecules (F4-TCNQ, PTCDA, TPA, $Na-NH_2$, $An-CH_3$, An-Br, Poly (ethylene imine) (PEI), and diazonium salts), and various biomolecules such as peptides, DNA fragments, and other derivatives. This is followed by a discussion on graphene-based gas sensor concepts. In reviewing the studies of the effects of molecular adsorption on graphene, it is evident that the strong manipulation of graphene's electronic structure, including *p*- and *n*-doping, is not only possible with molecular adsorbates, but that this approach appears to be superior compared to these exploiting edge effects, local defects, or strain. However, graphene-based gas sensors, albeit feasible because huge adsorbate-induced variations in the relative conductivity are possible, generally suffer from the lack of chemical selectivity.

Keywords: graphene, band gap engineering, surface modification, molecular adsorption, chemisorption

(Some figures may appear in colour only in the online journal)

1. Introduction

As has been widely discussed, the physical properties of graphene are unusual in several aspects and have led to extensive experimental and theoretical research efforts. Graphene is a 2D material with the largest known surface-to-volume ratio, and is related to the structurally-related carbon nanotubes [1–3]. It exhibits a high charge carrier mobility of up to $200\,000\,cm^2\,V^{-1}\,s^{-1}$ at electron densities of $\sim 2 \times 10^{11}\,cm^{-2}$ [4, 5], which is significantly higher than that of silicon ($<1,400\,cm^2\,V^{-1}\,s^{-1}$). The honeycomb lattice of graphene, now widely known and recognized (schematically shown in figure 1(*a*)), has a structural unit cell with a two-atom basis (the A and B sites), and is certainly not a Bravais lattice if the carbon atoms are regarded as identical. Each carbon atom

has one *s* and three *p* orbitals. Whereas the *s* and the two in-plane *p* orbitals do not contribute to the electric conductivity, the out of plane *p* orbitals hybridize to form valence and conduction bands, as shown in figure 1(*b*) [6]. What is important for some of graphene's properties is that both bands touch only at the high-symmetry points **K** and **K′** in the Brillouin zone, the Dirac points. Near these points the energy varies linearly with the momentum vector. In neutral graphene, Fermi energy separates the occupied and empty states at the Dirac points (figure 1(*c*)), thus making it a gapless semiconductor with almost no density of states at the Fermi level. Various approaches are known to change the charge carrier concentration, such as: Doping with charged impurities, applying an electric field, changing the temperature, and the adsorption of atoms and molecules. The electronic properties of graphene
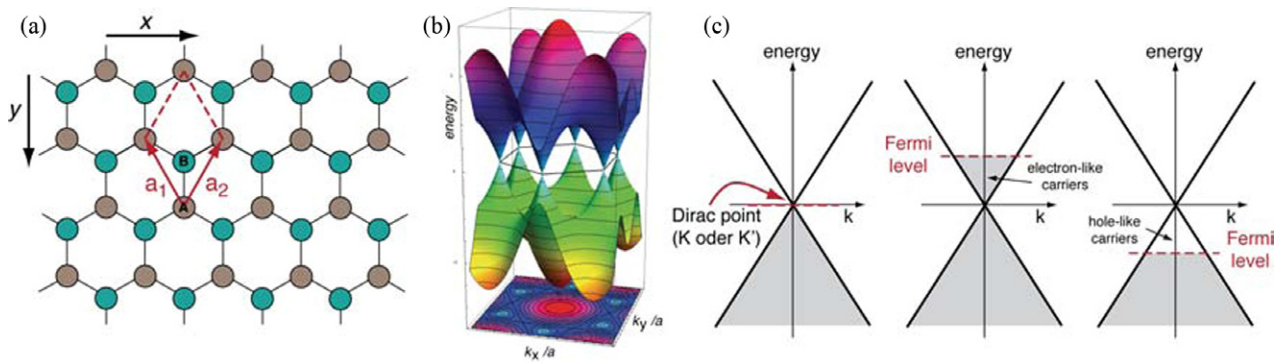
Figure 1. (*a*) The honeycomb lattice of graphene is described by a unit cell formed by the unit vectors a_1 and a_2 and a diatomic basis formed of atoms A and B (adapted from [6]); (*b*) the calculated band structure of graphene showing the occupied (yellow–green) and unoccupied (blue–red) states, which touch each other without energy gap at six K-points in the first Brillouin zone (image taken from [31]); (*c*) simplified band structure near the K points and Fermi level dependent charge carrier concentration. *N*- or *p*-type doping can create electron-like or hole-like charge carriers.

depend mainly on the band structure near **K** and **K′**, where the Dirac points occur at the Brillouin zone edge. While these changes in electron density are fairly small in absolute terms, in relative terms the doping of graphene through extrinsic (substrate or adsorbate interactions) or intrinsic effects (the doping of the graphene itself) can lead to huge changes in conductivity even as the carrier mobility changes.

When the Fermi level crosses the Dirac points where the density of charge carriers is zero [7], the conductivity should be very small. However, many experiments show that a residual conductivity remains despite the negligibly small density of states at the neutrality point, so that the electrical resistivity is never greater than a few kiloohms. This is, in part, a consequence of the behavior of electrons in graphene, which is identical to that of massless Dirac fermions. The ultrahigh mobility of the charge carriers in graphene and the excellent conductivity make it extremely appealing to substitute graphene for the current semiconductors (like Si) in electronic applications. But because of the absence of an electronic band gap, electronic devices based on graphene would be difficult to switch fully 'off.' In order to develop the graphene-based electronic devices that exploit graphene's outstanding electronic properties, a sizeable band gap will have to be engineered, while preserving the high charge carrier mobility.

Generally, a band gap in 2D sheets of graphene can emerge as a result of the interaction with some substrates, the introduction of atomic doping, or the adsorption of organic molecules [8–19]. However, the extent by which the band gap can be controlled through the substrate is very limited [8], while the induced defects have the disadvantage that they reduce the mean free path of the charge carriers and degrade the basic electronic structures of graphene. Extrinsic defects, caused by the substrate, corrugations of the graphene sheet, and short-range structural disorder, as well as intrinsic defects such as impurity atoms or ions, reduce the mobility of charge carriers in graphene [4, 20–26] and are difficult to control. By contrast, the adsorption of molecules on the surface of graphene can conveniently be controlled, while the damage to the structural electronic properties of graphene by the adsorbates is very limited. It has been frequently suggested that it is in fact

possible to modify the electronic structure of graphene without strong degradation of the ultrahigh mobility and destruction of the basic electronic properties through molecular adsorption [10–12, 14–17, 25–29]. Moreover, the adsorption of ordered overlayers of molecules with a large local dipole has been regarded as a potential route to the extrinsic placement of a charge density wave in graphene. Such a charge density wave could open a band gap in the graphene substrate. The charge carrier concentration can be affected significantly by the adsorbed molecules [11–19, 30]. An *n*-type doping of graphene can be easily obtained through the deposition of electron-donor molecules, while acceptor molecules can cause *p*-type doping [11–19] as shown in figure 1(*c*). For any deployment of adsorbate molecules in the functionalization of graphene as an electronic material, it is of fundamental importance to understand the interplay between the graphene surface and the adsorbate molecules, including the influence of adsorbates on electronic structure, band gap, resistance, electronic mobility, and doping type.

The purpose of this article is to review some aspects of the interaction of adsorbates, both large and small, with graphene and to provide an overview of the engineering of charge carrier concentration and the band gap in graphene using molecular adsorbates. This emphasis on adsorbate-driven properties distinguishes this review from others, which highlight aspects such as the current status and prospects of graphene [6, 32–35], electronic and photonic properties [36–39], graphene oxides [40], energy applications [41–43], and others [44–46]. The focus here is on epitaxial graphene (EG), and we explicitly exclude 1D graphene nanoribbons from this review, in which the electronic structure can be especially manipulated through edge modification. Also excluded are extensive discussions on the direct doping of graphene through the chemical modification of graphene itself, either by the introduction of defects or by elemental substitution of the carbon. Highlighted here will be interactions between the graphene surface and adsorbed molecules, including small gas molecules (H_2O, H_2, O_2, CO, NO_2, NO, and NH_3), and aromatic and non-aromatic molecules (F4-TCNQ, PTCDA, TPA, Na-NH_2, An-CH_3, An-Br, Poly (ethylene imine) (PEI),

Table 1. Results of first-principle calculations [11] compared to the experimental data obtained by Schedin *et al* [30]. E_α is the adsorption energy and ΔQ is the charge transfer to each carbon in the graphene [11].

Adsorbate	Theory	Expt.	E_a (meV)	ΔQ (e)
H_2O	Acceptor	Acceptor	47	−0.025
NH_3	Donor	Donor	31	0.027
CO	Donor	Donor	14	0.012
NO_2	Acceptor	Acceptor	67	−0.099
NO	Donor		29	0.018

and diazonium salts). This is followed by a discussion on various biomolecules in graphene.

Several potential applications have been proposed that follow directly from the sensitivity of graphene's electronic properties to adsorbates. Most importantly, graphene might be a suitable sensor for gasses and various molecules [30, 45, 47, 48]. Being an excellent conductor with extremely low electrical noise even within the limits of no free charge carriers, but with a large surface to volume ratio, the 2D structure of graphene maximizes the exposure area to gas molecules, and hence maximizes its ultimate sensitivity. Sensor concepts based on graphene are also reviewed in this article.

2. Small gas molecules

Since the pioneering demonstration of single molecule sensitivity of the properties of graphene using NO_2 and NH_3 by Schedin *et al* [30], the adsorption of small gas molecules such as H_2O, H_2, O_2, CO, NO_2, and NO, and their influence on the electronic structure and other properties of graphene have been reported [14, 17–19, 49–54]. First, it is clear that molecular adsorption (as alluded to in the introduction) can lead to either the *n*-type or *p*-type doping of graphene. First principle calculations for the adsorption of the small gas molecules H_2O, NH_3, CO, NO_2, N_2O_4 and NO on graphene show that NO_2 and H_2O always act as acceptors, while NH_3, CO, and NO act as donors [11, 12]; this is in agreement with experiment, as shown in table 1. Interestingly, while NO_2 causes a relatively strong *p*-type doping, the relatively similar NO molecule causes *n*-type doping. This difference is the result of the interplay of charge donation and back-donation between the graphene and the adsorbates [11]. Yet, compared to the strong acceptor character of NO_2, the dimer N_2O_4, which naturally occurs in the equilibrium gaseous state, just acts as a weak donor and so no significant doping effect was found for the N_2O_4 adsorption on graphene [52, 53].

It should be noted that the adsorption of NO_2 shows a very limited effect on the mobility of charge carriers in graphene [30]. The parallel shift in conductivity versus voltage curves for graphene as a result of adsorption, as shown in figure 2, implies that the entire adsorption and desorption process does not significantly affect the high mobility of graphene, similar to what is found for the adsorption of H_2O and O_2 [15], in which case the carrier density in graphene was $4 \times 10^{12}\,e\,cm^{-2}$ after adsorption [14, 54].

The interaction between the small adsorbed molecules and graphene is further complicated, not only by the choice
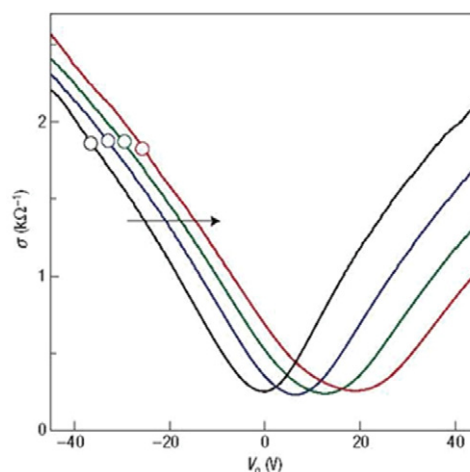
Figure 2. Conductivity of single-layer graphene as a function of gate voltage. The parallel shift is due to the increase of NO_2 doping from zero (black curve) to ~$1.5 \times 10^{12}\,cm^{-2}$ (red curve). NO_2 doping adds holes and induces charged impurities. The parallel shift of $\sigma(V_g)$ implies a negligible scattering effect of the charged impurities by the chemical doping. Also the Hall mobilities of electrons and holes are not affected by chemical doping. Figure reproduced with permission from [30].
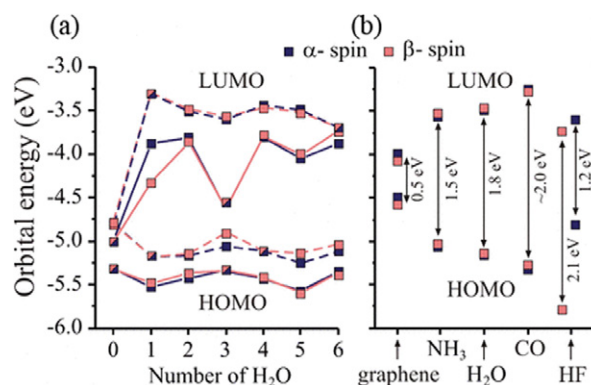
Figure 3. Effect of adsorption on the gap in nanoscale graphene. (*a*) The HOMO and LUMO energies for graphene of size $N = 3$ (solid line) and $N = 5$ (dashed line) versus the number of adsorbed water molecules. (*b*) Influence on adsorption of different adsorbed molecules on the bandgap of the nanoscale graphene of size $N = 4$ [55].

of adsorbate, but also by both the orientation of the adsorbed molecules with respect to the graphene surface and the structure of the graphene itself (pristine, doped, or defected [12]). For instance, Leenaerts *et al* [11] suggest that there is almost no charge transfer between graphene and NH_3 when the H atoms are pointing towards the graphene surface. On the other hand, the charge transfer is about 0.03e when the H atoms are pointing away from the graphene surface, since in this latter orientation of ammonia, its highest occupied molecular orbital (HOMO) is the only one that has a significant overlap with the graphene orbitals. The investigation of the band gap induced by different adsorbed molecules by Berashevich *et al* [55] indicates that the band gap resulting from the adsorption of NH_3, H_2O, CO, and HF can be up to ~1.5 eV–2.0 eV, as a result of both the symmetry breaking of the sublattice and the molecular symmetry of graphene, as seen in figure 3.
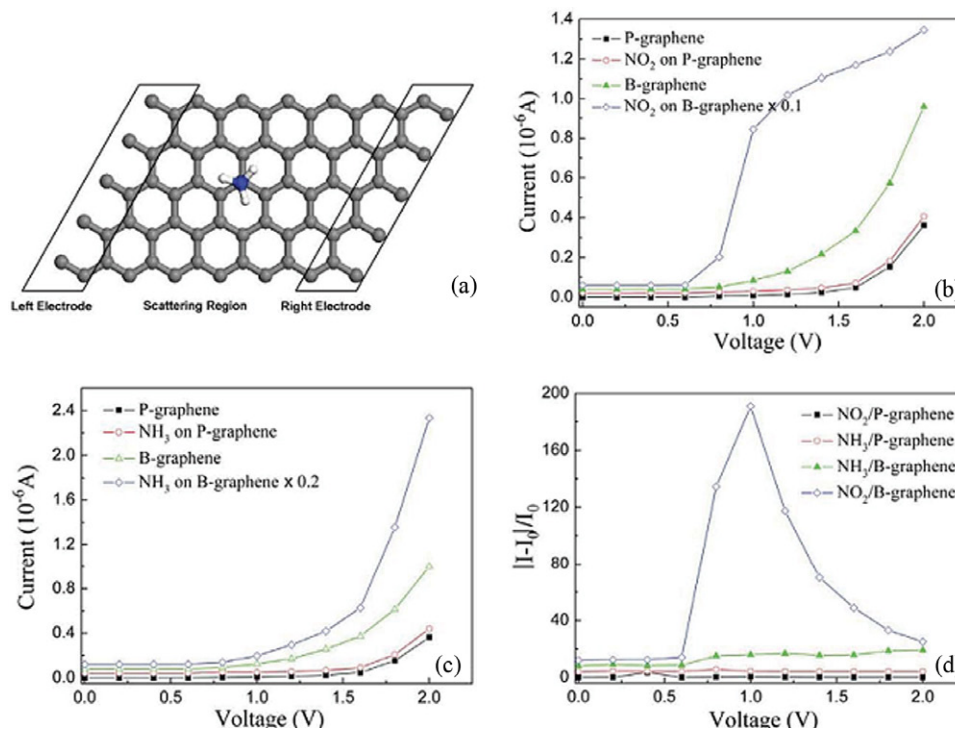
Figure 4. A schematic of the graphene-based chemical sensor used to detect small gas molecules (*a*). The comparison of NO_2 and NH_3 adsorption on pristine (*P*-graphene), and boron doped (*B*-graphene) based devices (*b*, *c*, *d*), reproduced with permission from [12].

All of this is just what is believed to be the case for a pristine and nearly perfect graphene; for a defective graphene the situation becomes even more complex. The adsorption of small gas molecules on doped or defective graphene may well be much stronger than on a pristine graphene, as implied by the I-V curves taken for pristine, doped, or defective graphene electronic junctions by Zhang *et al* [12], as shown in figure 4. For instance, the sensitivity of the boron-doped graphene (*B*-graphene) to small gas molecules (NO_2 and NH_3) is much higher than that of the pristine graphene (*P*-graphene) due to the increased hole-type charge carriers in boron-doped graphene. This suggests that the graphene-based gas sensors might be significantly improved by introducing suitable dopants or defects in graphene [12]. In addition, an analysis of the adsorbed gas molecules on transition metal embedded graphene showed that the introduction of transition metal elements, especially Ti and Au, can significantly enhance the interactions between gas molecules and graphene [49]. These results are consistent with several other studies [56–58]. Of course, as noted above, these intrinsic defects will significantly lower graphene mobility.

As is evident from the discussion above, adsorbates will dope graphene. To realize improved semiconductor properties, it is not enough to simply open up a band gap in the electronic structure of graphene, i.e. modify graphene though adsorbate interactions from a gapless semiconductor to a 'proper' semiconductor with a well-defined band gap. As charge donation may also accompany the band gap modification that occurs with adsorbate interactions, the Fermi level may not fall within the gap formed in graphene. So the potential device benefits, say better on–off ratios in a transistor geometry, in which graphene is the narrow channel semiconductor, will

not always occur. Significant band gaps can nonetheless be obtained through adsorbate interactions. This is even true of the most simple of adsorbates such as hydrogen, as will be discussed in the following section.

The complications associated with small molecule adsorption, as far as graphene device operations go, is that the type and extent of molecular adsorption could very well be sensitive to ambient conditions, and those conditions may vary strongly. The adsorbed molecules can be completely removed by desorption under certain conditions. Schedin *et al* [30] showed that the adsorbed molecules (H_2O, NH_3, CO, and NO_2) can be completely desorbed by annealing at 150 °C. This finding has also been confirmed by other groups [14, 54]. This can be very useful in a device as it helps restore its initial state.

2.1. H_2 adsorption on graphene

The hydrogenation of graphene has been extensively studied both theoretically and experimentally [59]. The opening of a band gap through hydrogenation was achieved, for instance, through the patterned adsorption of hydrogen atoms on graphene / Ir(111 [19]), as shown in figure 5. For a completely hydrogenated suspended graphene layer, calculations by Sofo *et al* [60]. suggest that the chemisorbed hydrogen atoms are bonded to carbon on both sides of each graphene layer. Thus, the hybridization state of graphene is transformed from sp^2 to sp^3 forming a hexagonal network, therefore, π and π^* orbitals change to σ and σ^*. This leads to a 3 eV band gap. As such, graphene turns out to be useful for H_2 storage. The C–H bonds in the hydrogenated graphene can be broken under certain conditions and thus the adsorbed hydrogen atoms can be
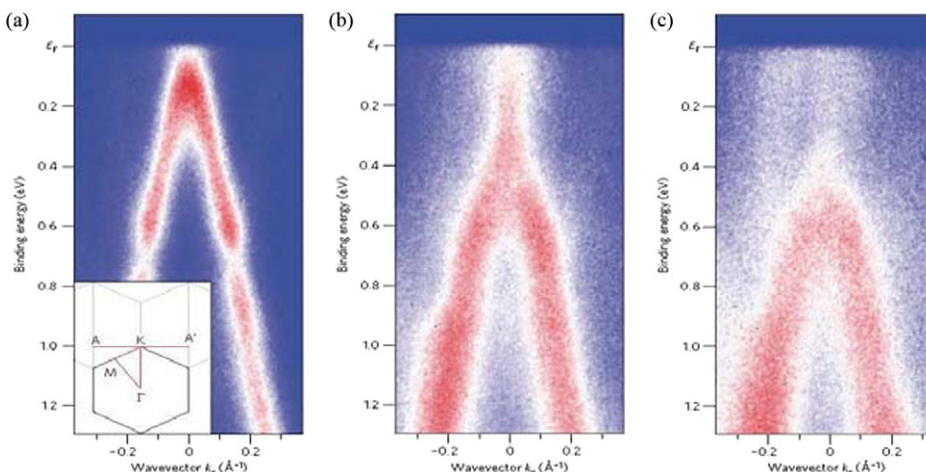
Figure 5. Change in the π–band of graphene on Ir(1 1 1) with increasing H_2 exposure, reproduced with permission from [19].
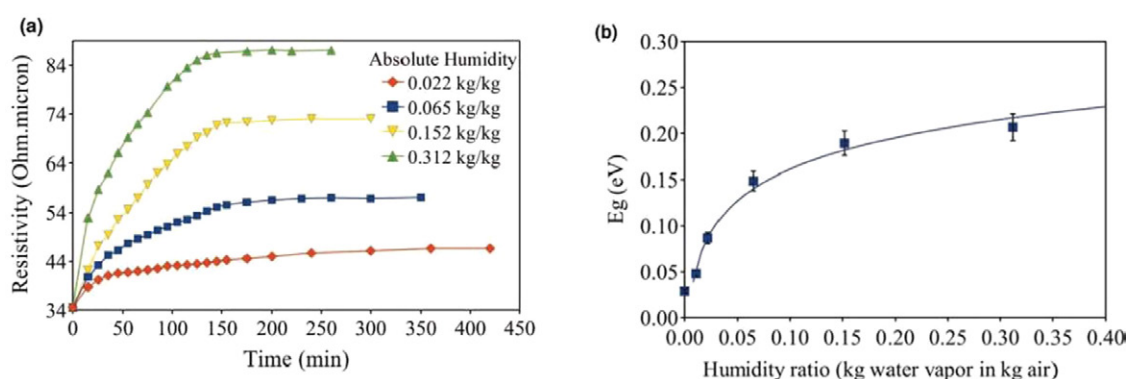
Figure 6. Resistivity and band gap change of graphene due to the adsorption of water, reproduced with permission from [50].

released [54]. It was demonstrated that ~5 wt% of hydrogen atoms can be chemically stored in just a few layers of graphene, while the storage of hydrogen in carbon nanotubes is significantly less, around 3 wt% [61–63]. Given the long history of carbon black being used as a hydrogen storage media, the potential applicability of graphene for hydrogen storage may not be surprising.

Similar to the case of hydrogen adsorption, where each hydrogen molecule bonds to one carbon atom, also F_2, HF, and HCl adsorption is expected to result in this complete coverage on graphene [64]. The model studies of Boukhvalov and Katsnelson [64] revealed that F_2 can produce a homogeneous structure with a large band gap but weak disorder and yet can retain high mobility. The chemisorption of HF, by comparison, requires a large amount of energy, and hence it is very stable with respect to graphene at room temperature. The interaction between HCl and graphene is very weak, only dominated by van der Waals forces, and may be worth further exploration because the bond length of HCl (1.27 Å) is close to the carbon–carbon bond length of graphene. The HCl molecules are believed to just hover over the graphene layer through van der Waals force and no molecular dissociation occurs from the interaction with graphene [64]. But it is not only small molecules such as HCl that interact with graphene largely via dispersive forces alone, adsorbates such

as water and oxygen act very similar in that regard, as discussed below.

2.2. H_2O adsorption on graphene

Graphene is always found to be p-doped as the result of H_2O and O_2 adsorption in air [13–15]. Furthermore, a band gap opening in graphene is also induced by the exposure to water molecules [50]. The dipole moment of H_2O is key: spin-polarized density-functional theory showed that a band gap of up to ~2 eV is induced by water molecule adsorbates if the dipole moment of the water molecules is directed towards the graphene, however it is only a ~0.8 eV band gap if the same dipole moment is directed away from the graphene [55]. Experiments confirmed that the band gap increased with the level of humidity and achieved 90% of the saturation value of 0.206 eV with a humidity level of 0.312 kg of water per kg of air (figure 6 [50]). The water molecules are more likely adsorbed in the center of the carbon rings and on a bridge site between two carbon atoms. This is in striking contrast to ammonia, atomic hydrogen, fluorine and chlorine adsorption which are believed to prefer top adsorption sites.

A study on water–graphene interactions by Rafiee *et al* shows that graphene as a coating does not significantly alter the wetting behavior of surfaces, as shown in figure 7 [65].
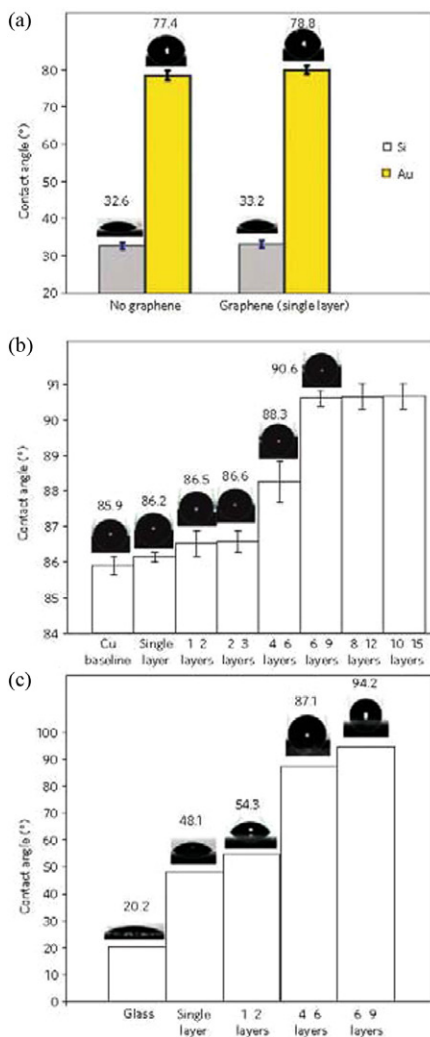
Figure 7. Wetting transparency effect of graphene on (*a*) Si, Au and (*b*) Cu substrates, but not on (*c*) glass substrate, reproduced with permission from [65].

Such a small influence of graphene on wetting, which can be considered as a 'transparency' to surface wetting, is ascribed to its atomically thin nature, structural homogeneity and chemical inertness. This suggests that graphene can be an ideal coating material. Support of this conclusion comes from a study of the hydration of graphene [66], which also showed that water molecules could not penetrate a graphene film [67]. Even hydroxyl ions are too large to penetrate the graphene film, so that they form water molecules on the surface of the graphene instead.

2.3. NH₃ adsorption on graphene

Several experimental studies demonstrated that NH$_3$ adsorption typically causes *n*-type doping of graphene [13–16]. Theoretical studies show that NH$_3$ is one of the largest electron donors, with a large amount of electron transfer to graphene (0.03e), in comparison to other electron donor molecules such as CO [11, 12], but as noted, the adsorption geometry matters. NH$_3$ adsorption predominantly occurred on the defect sites and the edges of graphene where the activation barrier is relatively low [13, 68]. The

level of *n*-type doping was systematically increased by increasing the defect density in the graphene film through gas phase oxidation [13, see erratum]. This is similar to the adsorption of NH$_3$ on SWNT, which mainly happens at wall defect sites [69]. The formation of carbon–nitrogen bonds was confirmed by x-ray photoelectron spectroscopy and nanometer-scale secondary ion mass spectroscopy of graphene by Wang *et al* as shown in figure 8 [13]. The graphene was thermally annealed in ammonia and argon, for comparison. The occurrence of an N signal and a much larger CN/C$_2$ ratio were observed for NH$_3$ exposure only. Moreover, the interaction between ammonia and graphene through the formation of multiple *p-n-p* junctions appeared to be strongly dependent on the thickness of the graphene layers, as demonstrated by Antonova *et al* [16]. Few layer graphene flakes were found to show extremely high response to ammonia adsorption, 1–8 orders of magnitude higher than that of single layer of graphene [16].

Ammonia molecules adsorbed on graphene/Ni(1 1 1) heterosystems were observed to be adsorbed on top of the carbon atom [70], much like what was found for atomic hydrogen, fluorine, and chlorine adsorption.

3. Planar molecular adsorption and graphene modification

Larger, planar molecules can act as electron donors or acceptors, and change the conductivity through a change in the density of free carriers, and even create and manipulate a band gap. For example, Raman G-band splitting was observed in some aromatic molecules dispersed on graphene [70–76]. The sp^2- bonded carbon network of graphene is disrupted by forming covalent or non-covalent bonds with the adsorbate, thus breaking the symmetry of graphene and opening up a band gap. As is commonly observed, the width of the band gap is dependent of the adsorbate coverage.

Adsorbate molecules can form either covalent or noncovalent bonds with graphene. For instance, some strong acids and oxidants can significantly disrupt the sp^2-bonded carbon network of graphene and functionalize the graphene by forming covalently attached hydroxyl and epoxide groups [76]. Molecules with epoxy groups are easily attached to the edge and defects of graphene through C–O bond formation [77]. On the other hand, the ring structure of aromatic and non-aromatic molecules, including DNA and proteins [78], can cause their attachment to graphene through non-covalent bonds, such as π–π interactions or van der Waals interactions. It will be discussed in this section that the degree of the modification on the electronic structure of graphene generally depends on the balance between adsorbate–adsorbate interactions and adsorbate–graphene interactions. In addition, the adsorption of organic molecules can also be dramatically enhanced by the inclusion of metal atom dopants into graphene [79, 80].

3.1. Benzene

A large number of both theoretical and experimental studies of the adsorption of benzene, naphthalene and their various
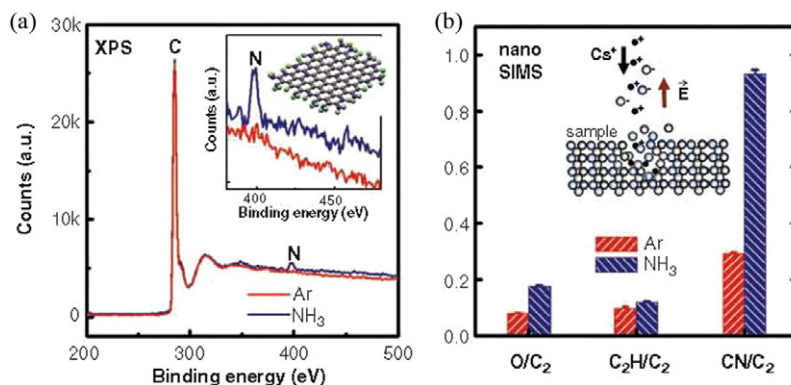
Figure 8. Spectroscopy of a gas-phase oxidized graphene sheet, thermally annealed in NH_3 and Ar. The sample annealed in NH_3 shows a clear N signal, whereas the control sample does not (inset). Right: the sample annealed in NH_3 has a much higher CN/C_2 ratio indicating the formation of more C–N bonds than is evident in the control samples, reproduced with permission from [13].

substituted derivatives on graphene have been performed [74, 79–84]. Both benzene and naphthalene molecules bind very weakly, or do not bind at all, to graphene sheets in the planar stack orientation (figures 9(*b*) and (*d*) [74, 79–82]). The adsorption energy of benzene molecules is typically very low, less than 0.2 eV. It has been established that there is no significant charge transfer between benzene / naphtalene and graphene, and that the electronic structure of graphene is only weakly perturbed by these adsorbates, unless the benzene is placed very close to the graphene [84]. Indeed in the case of close proximity and strong covalent bonding [84], a band gap would be present although it must be recognized that such strong covalent bonding is unlikely. Exceptions that could lead to strong benzene interactions with graphene would require a more complex adsorption system, like a lithium interlayer [85]. However, the presence of functional groups can significantly change the overall π–π interactions between the adsorbed molecules and graphene and the adsorption energy can be increased significantly when some specific groups are added to the aromatic core, for example NH_2 groups or COOH groups [74, 79–82].

Other benzene derivatives, such as *p*-nitrophenyl, will covalently bond to graphene, thereby causing a change in conductivity and surface potential [86–88]. A band gap in graphene of approximately 0.36 eV was observed by angle-resolved photoemission spectroscopy for diazonium ((*p*-nitrophenyl) diazonium tetra–fluoroborate) functionalized epitaxial graphene [89]. This was ascribed to the partial conversion of sp^2—hybridized carbon to sp^3 [89].

Generally, diazonium salts not only covalently bond to graphene but are electron acceptors, causing *p*-doping of the graphene [90–92]. Similarly, reversible electrochemical naphthylmethyl attachment to graphene has been demonstrated and also seen to be reversible [93].

3.2. The Diels–Alder reaction functionalization of graphene

Covalent bonds with graphene are by no means limited to the formation of one sp^3 bond, but pericyclic reactions between ethylene, butadiene, 2,3-dimethoxybutadiene and 9-methylanthracene [94] are possible. Indeed,
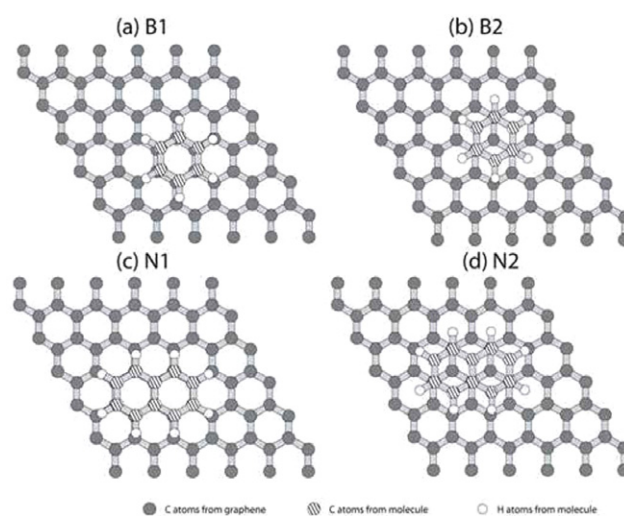
Figure 9. Top view of the optimized structures of (*a*) hollow and (*b*) stack sites for benzene/graphene and (*c*) hollow and (*d*) stack sites for naphtalene/graphene, reproduced with permission from [80].

the Diels–Alder reactions with graphene are allowed and observed [94]. Tetracyanoethylene (TCNE), discussed below further, will also undergo a pericyclic Diels–Alder reaction with graphene [95].

3.3. F4-TCNQ, TCNQ and TCNE adsorption

Both tetracyanoquinodimethane (TCNQ) and its fluorinated derivative F4-TCNQ are widely used electron acceptors, applied for instance in organic solar cells. Both molecules have four strong electron-accepting cyano groups, but F4-TCNQ has the higher electron affinity (E_{ea}=5.24 eV, as opposed to 3.22 eV for TCNQ [96–98]). Similar to the adsorption mechanism of benzene on graphene, TCNQ and TCNQ derivatives adsorption on graphene and various metals have been widely studied [99–108]. TCNQ and F4-TCNQ molecules are arranged in a planar orientation on a graphene substrate [96]. Because of its higher electron affinity, F4-TCNQ is the stronger electron acceptor [70] having a *p*-doping effect on graphene. Theoretical and experimental analyses successfully show that
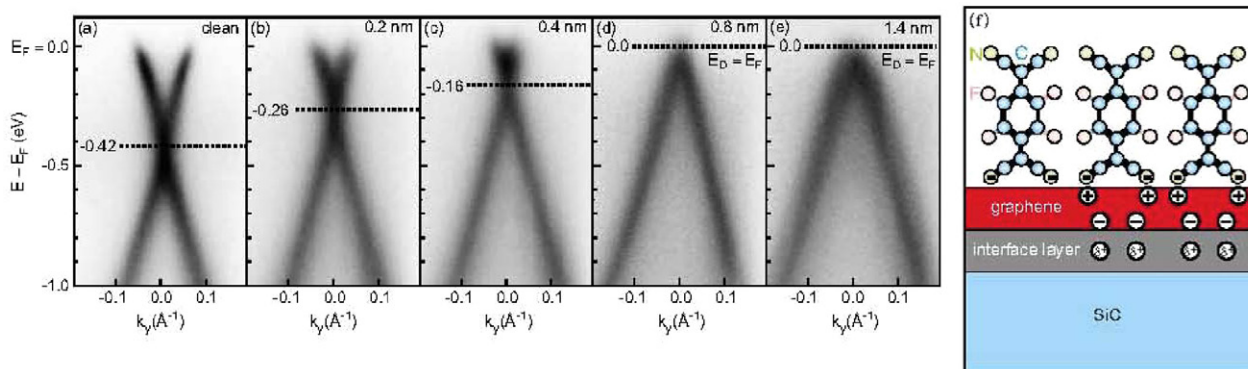
Figure 10. Dispersion of the p-bands of graphene/SiC(0 0 0 1) around the $\overline{K}$ point of the graphene Brillouin zone, as function of coverage with F4-TCNQ. The Fermi level E_F of the uncovered graphene is offset from the Dirac point (E_D, dashed line) due to excess negative charge, which is gradually compensated with F4-TCNQ coverage. Charge neutrality ($E_F = E_D$) is reached for a molecular coverage of 0.8 nm [70].
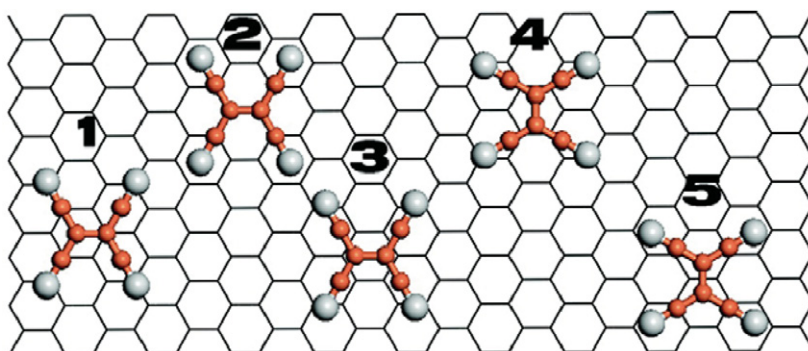
Figure 11. Schematic top view of the TCNE on graphene showing five high-symmetry adsorption sites, reproduced with permission from [53], copyright (2009) American Chemical Society.

both the doping level and the magnitude of the band gap can be controlled by the adsorption of the F4-TCNQ [70, 98, 109, 110]. With increasing adsorbate concentration of F4-TCNQ, the Fermi level of graphene shifts progressively towards the Dirac point, as illustrated in figures 10(a)–(e). Also revealed is that the band gap in graphene, if engineered by SiC/graphene interface dipoles, increases with F4-TCNQ coverage. This was attributed to the increased electrostatic field caused by the additional dipole developing at the graphene/ F4-TCNQ interface, as shown schematically in figure 10(f). This is a clear demonstration that the magnitude of the graphene band gap can be modified by controlling the amount of molecule doping.

Similarly to TCNQ and F4-TCNQ, tetracyanoethylene (TCNE) also has four strong electron-accepting cyano groups (figure 11) and a large electron affinity, and thus acts as a strong electron acceptor. The adsorption of TCNE also results in significant p-type doping. Again, the doping level increases with the coverage of the TCNE molecules [53, 78, 110], and a band gap is induced by TCNE.

3.4. TPA, Na-NH₂, An-CH₃ and An-Br adsorption

Although the adsorption of both benzene and naphthalene did not lead to a band gap opening in graphene, the electronic structure of graphene can be significantly modulated through strong π–π interaction between the aromatic molecules tetrasodium

1,3,6,8-pyrenetetrasulfonic acid (TPA), 1,5-naphthalenediamine (Na-NH₂), 9,10-dimethylanthracene (An-CH₃) and 9,10-dibromoanthracene (An-Br), shown in figure 12, and the graphene layer. It was suggested by Dong *et al* that this is the result of the addition of functional groups [71]. It is revealed that the ratio of the intensities of the 2D band at 2696 cm⁻¹ and the G band at 1585 cm⁻¹, I(2D)/I(G), significantly decreased, and that the Raman D band at 1354 cm⁻¹ occured after the deposition of TPA molecules on the top of graphene. This clearly demonstrates a doping effect and an increasing effective disorder of the graphene layer [71]. The Na-NH₂ and An-CH₃ molecules can cause n-type doping, acting as an electron donor, whereas An-Br and TPA act as acceptors and induce p-type doping on a single layer graphene. This is in parallel to an upshift of the Raman 2D and a down shift of the G-band for An-Br adsorbed on graphene, as well as an upshift of both Raman G and 2D bands for TPA adsorbed on graphene. Furthermore, the Raman G-band of TPA-dispersed graphene was found to be split into two distinct peaks due to the removal of the two-fold energy degeneracy of the two optical phonon modes (LO and TO) at the Γ point [111]. However, except for the symmetry breaking, the calculated phonon dispersion curves of TPA-dispersed graphene are similar to that of the pristine graphene, and are in agreement with the experimental D band frequencies. This indicates that the other Raman features (D and 2D) are not significantly affected [111]. A similar
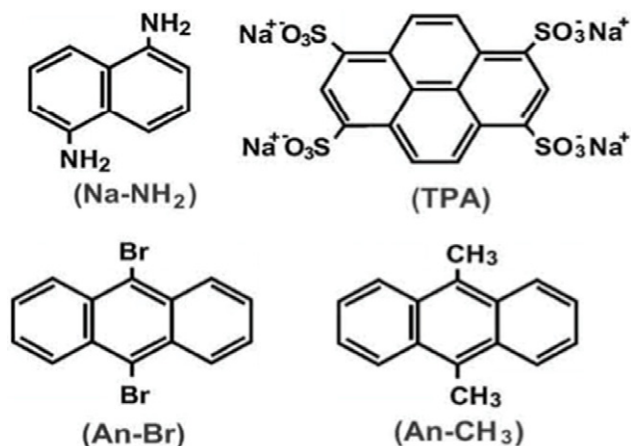
Figure 12. Chemical structure of Na-NH$_2$, TPA, An-Br, An-CH$_3$

Figure 13. Raman G band splitting of different molecules-dispersed graphene [111].

G-band splitting was also observed in other aromatic molecules dispersed on graphene, such as pyrene, anthracene, and naphthalene. The G-band splitting induced by different aromatic molecules (figure 13) implies that the splitting increases with a larger aromatic ring size. Consequently, a band gap should be induced as a result of such symmetry breaking.

3.5. PTCDA and VOPc adsorption

In order to form a high quality oxide film on top of graphene, many studies have focused on the growth of the organic semiconductor 3,4,9,10-perylene tetracarboxylic dianhydride (PTCDA) on epitaxial graphene on SiC [112–115]. The rationale here is that PTCDA has already been extensively investigated as a model system for organic or inorganic interfaces and is known to form ordered structures on various substrates [116, 117]. The scanning tunneling microscopy (STM) image in figure 14 from [113] shows that a continuous, highly ordered PTCDA monolayer, which is lying flat on epitaxial graphene, is formed in a herringbone arrangement. This herringbone structure of the PTCDA layer is quadrupolar and stabilized by hydrogen bonding. The interactions between the PTCDA molecules are thus much stronger than the interfacial interaction between PTCDA and graphene. Studies by several authors [112–115] suggested that the π–π* interactions bind the molecules to the graphene surface. The PTCDA layer appears to be unperturbed by graphene defects and atomic steps of the SiC substrate. Moreover, the particularities of the electronic properties of the PTCDA monolayer and the absence of any new peaks or binding energy shifts in high-resolution photoelectron spectroscopy measurements further confirmed that the interaction between PTCDA and graphene is weak [112]. This is consistent with theoretical results [118]. With regards to doping, the adsorbed PTCDA molecules gain electrons, causing *p*-type doping in the graphene.

In addition, the comparison between the adsorption of 2-phenyl-4,6-bis(6-(pyridin-3-yl)-4-(pyridin-3-yl)pyridin-2-yl)pyrimidine (3,3′-BTP) and PTCDA on graphene/Ru(1 0 0) shows that a 2D adlayer phase was formed by PTCDA adsorbates due to the strong intermolecular interaction, while linear or ring-like structures were formed by 3,3′-BTP adsorbates. The latter shows the influence of adsorption potentials related to the graphene corrugation, since here intermolecular interactions are significantly weaker than the potential energy corrugation of the surface.
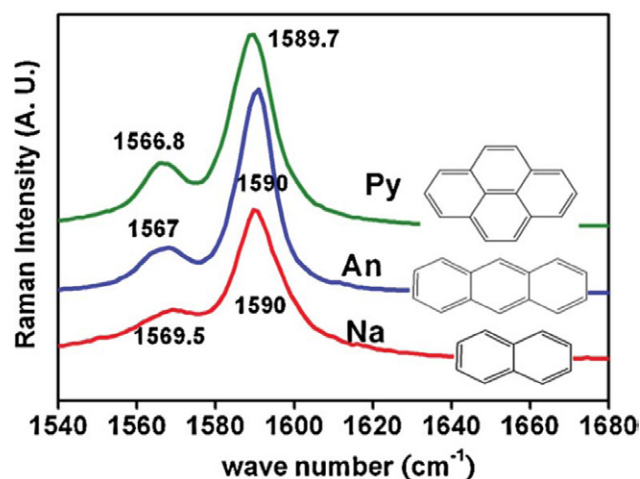
Vanadyl-phthalocyanine (VOPc), by itself a *p*-type organic semiconductor, has been tested as adsorbate on graphene. Layers of VOPc on few-layer graphene were studied with atomic force microscopy (AFM) and Kelvin probe force microscopy (KPFM) (figure 15 [109]). Transport measurements in a field-effect transistor (FET) configuration, fabricated from VOPc-modified graphene, revealed slight *n*-type surface doping, where the mobility was determined to 2000–3000 cm^{2}V^{-1}s^{-1}, with an on–off ratio of about 1.4 [109].

3.6. Interaction with 2,4′ BTP

The adsorption behavior and structure formation of organic molecules 2,4′-bis(terpyridine) (2,4′- BTP) (figures 16(*a*) and (*b*)) on graphene adlayers grown on Ru(0 0 0 1) was found to be dominated by a pronounced lateral variation of the molecule—substrate interactions [119], which are a result of the corrugation, or buckling, of the epitaxial graphene layer. The 2,4′ BTP adsorbates, albeit large compared to this buckling, find their preferred adsorption sites in the valleys of the graphene. As a result, separated 1D chain structures of 2,4′ BTP were formed, as is evident from the STM images in figures 16(*c*) and (*d*). By comparison, on the crystalline and flat surface of Ag/Ru(0 0 0 1), i.e. in the absence of a corrugated adsorption potential, the intermolecular interactions between chains dominate so that a 2D network structure is adapted (figure 16(*d*)).

4. The adsorption of planar molecules with large intrinsic dipoles

The adsorption of molecules with strong intrinsic dipole has been studied in the context of the polarization control
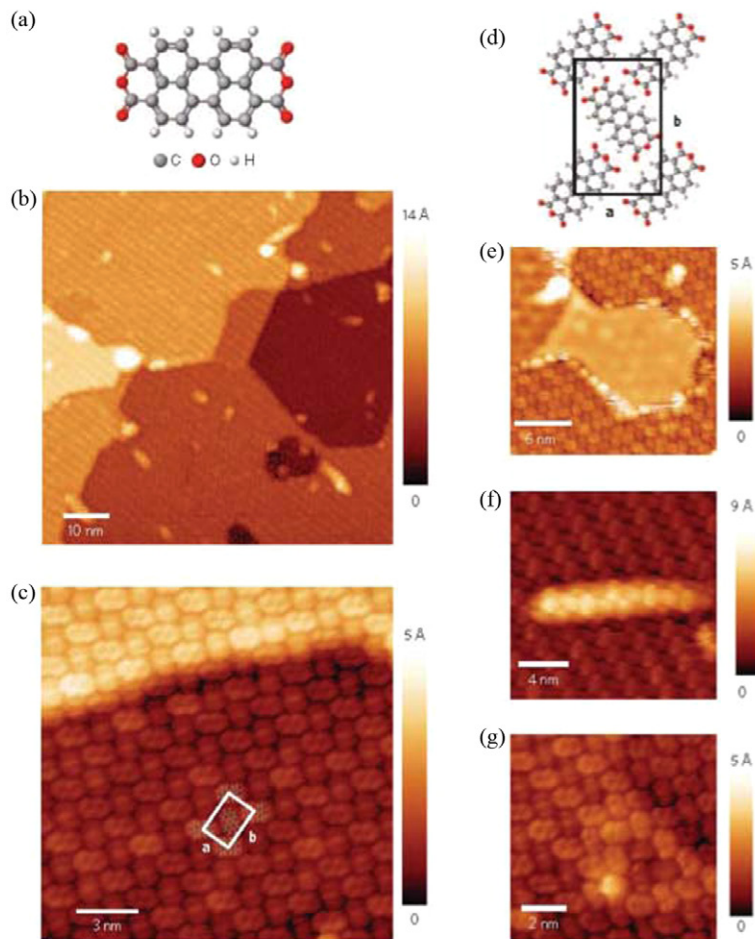
Figure 14. PTCDA molecules and STM images of PTCDA on graphene/SiC. Adopted with permission from [113].
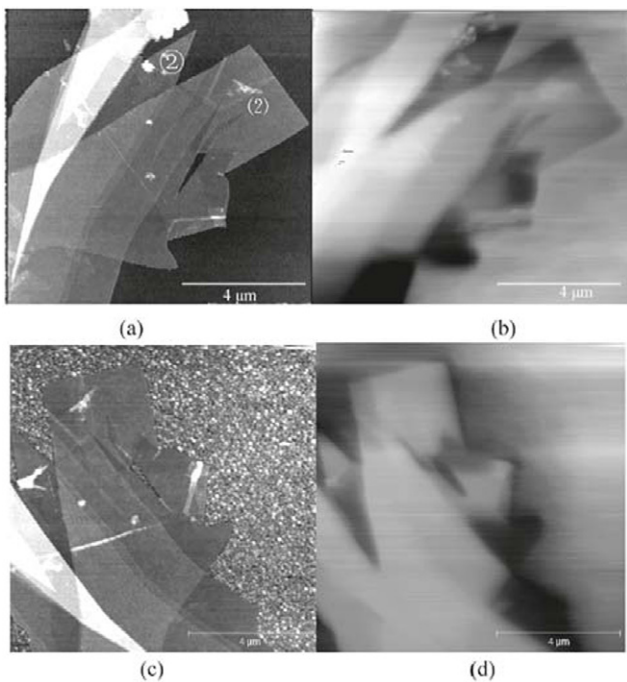
Figure 15. AFM and KPFM images of vanadyl-phthalocyaninen (VOPc)—doped on few-layer graphene. (*a* and *c*) AFM before and after doping. (*b* and *d*) KPFM before and after doping, reproduced with permission from [109], copyright (2011) American Chemical Society.

of physical and chemical properties, such as surface magnetism and electric surface polarization. The fundamental idea is to exploit the electric field emerging from the molecular dipole to perturb or modify locally the electronic structure of the material to which the adsorbates attach, through a Stark effect, charge screening and related polarization-induced effects. With regards to dipolar molecule adsorption on graphene, it is reasonable to expect that an ordered layer of such adsorbates would generate a charge density wave in graphene, potentially causing an opening of a band gap. Factors determining the interaction between dipolar molecules and graphene are the strength and nature of the adsorbate/graphene interaction, chemical inertness of the graphene, the amount of charge screening and the effect of local dipoles on the charge carrier mobility through the creation of extrinsic impurity-like scattering centers. As has been shown before [8], experiments, such as direct and inverse photoemission, are able to assess the cumulative effect on the band structure of graphene. Indications of the role of the molecular dipole have already been seen in section 2 for small adsorbates.

4.1. Zwitterionic molecular adsorption

The investigation of the adsorption of molecules with large dipole on gold and graphene/copper was carried out recently
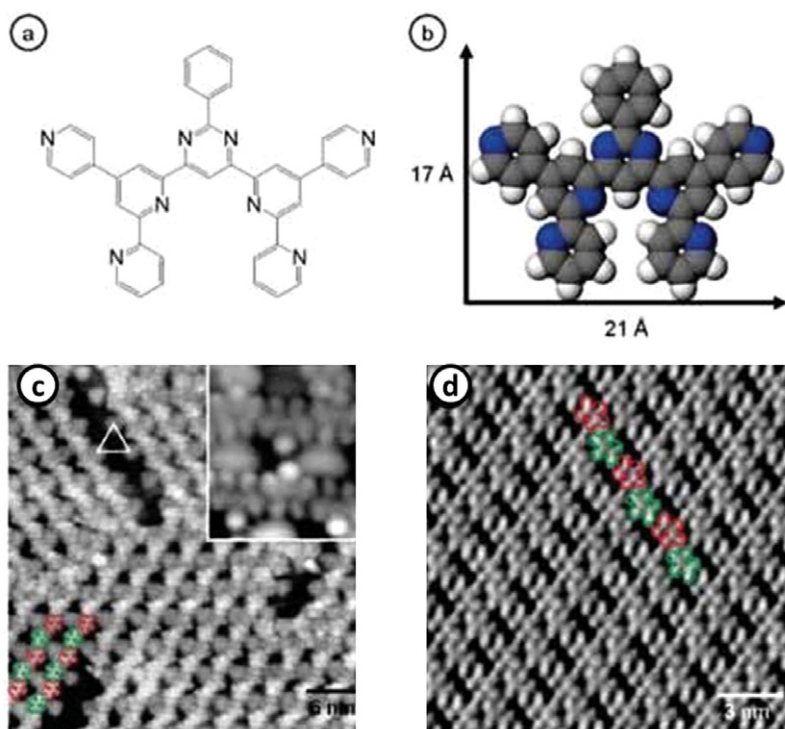
Figure 16. 2,4′- BTP molecules (*a* and *b*) and the STM image of 2,4′- BTP molecules on graphene/Ru(0001) (*c*) and on Ag/Ru(0001) (*d*), reproduced with permission from [119].
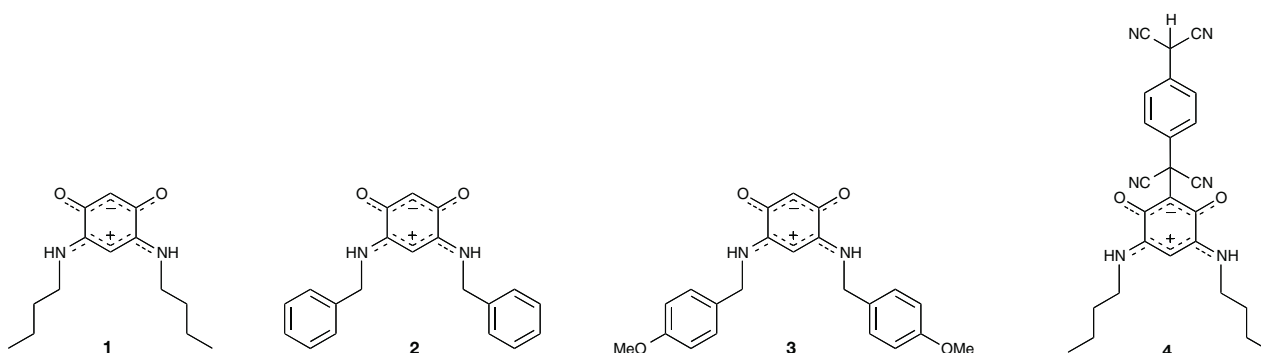
Figure 17. The zwitterion *p*-benzoquinonemonoimine (6Z)-4-(butylamino)-6-(butyliminio)-3-oxocyclohexa-1, 4-dien-1-olate, $C_6H_2(\cdots NHR)2(\cdots O)_2$ where R = butyl **1**, benyzl **2**, methoxy benzyl **3**, and the TCNQH functionalized *p*-benzoquinonemonoimine zwitterion, where R = butyl **4**.

[120]. These studies were focused on *p*-benzoquinonemonoimine zwitterions of type $C_6H_2(\cdots NHR)_2(\cdots O)_2$, as shown in figure 17, because of their zwitterionic ground state [121–125]. The molecules, although electrically neutral as a whole, carry positive and negative charges on opposite parts of the C_6 ring 'core,' resulting in a large dipole moment of approximately 10 Debye (D). A comparison of the quinonoid zwitterion adsorbed on both gold and graphene shows that the photoemission and inverse photoemission final states are much more weakly screened for dipolar molecules **1** and **3** on graphene than that on gold, see figure 18. This is evident in the much larger HOMO to the lowest unoccupied molecular orbital (LUMO) gap for the molecules on graphene than that on gold. In addition, the study shows that there is no significant change in the graphene Raman peak position and relative intensities with the adsorption of the quinonoid zwitterion molecules (figure

19). This implies that the response of the graphene on the adsorbed quinonoid zwitterion molecules is very weak. This observed difference in response, between Au and graphene, to zwitterion adsorption is expected to be due to the very different chemical bonding and different hybridization. The *p*-benzoquinonemonoimine zwitterion, (6Z)-4-(butylamino)-6-(butyliminio)-3-oxocyclohexa-1, 4-dien-1-olate, of formula $C_6H_2(\cdots NHR)_2(\cdots O)_2$ where R = *n*-C_4H_9 (molecule **1** in figure 17) is known to 'stand up' with the plane of the zwitterion molecular core normal to the surface, when the deposition from solution onto gold occurs [121]. But studies of various *p*-benzoquinonemonoimine zwitterions [126], deposited from solution on graphite, suggest that the molecules lie 'flat' on the graphite surface, similar to tetracarboxylic dianhydride (PTCDA) molecules on epitaxial graphene on SiC ([112–115] and section 3.5), where the interaction between the PTCDA
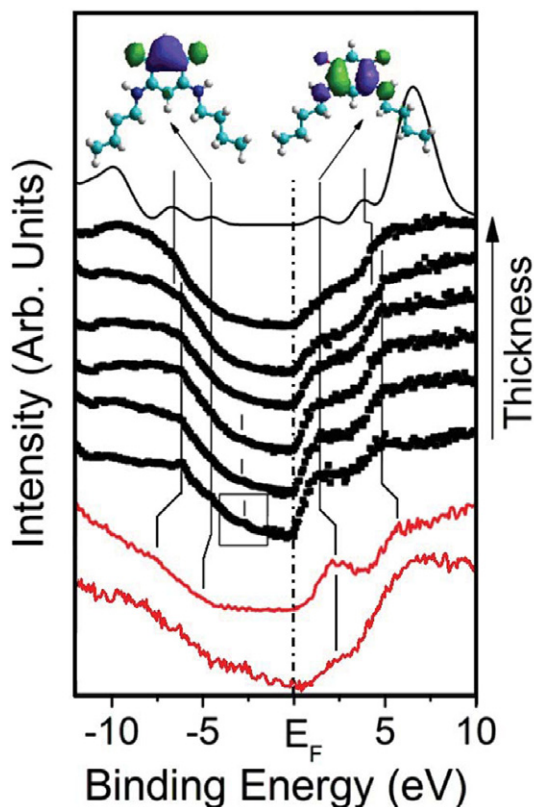
Figure 18. Comparison of the combined photoemission (left) and inverse photoemission (right) spectra (thick lines) of the *p*-benzoquinonemonoimine zwitterion, (6Z)-4-(butylamino)-6-(butyliminio)-3-oxocyclohexa-1, 4-dien-1-olate, of formula $C_6H_2(\cdots NHR)_2(\cdots O)_2$ where $R = n$-C_4H_9, adsorbed on Au (black) and graphene on copper (red) as a function of coverage, reproduced with permission from [120].

Figure 19. Comparison of the D, G and 2d peaks in the Raman spectra (*a*) graphene, (*b*) *p*-benzoquinonemonoimine zwitterion, (6Z)-4-(butylamino)-6-(butyliminio)-3-oxocyclohexa-1,4-dien-1-olate (molecule **1** of figure 17), of formula $C_6H_2(\cdots NHR)_2(\cdots O)_2$ where $R = n$-C_4H_9, adsorbed graphene on copper and (*c*) *p*-benzoquinonemonoimine zwitterion, (6Z)-4-(benzylamino)-6-(benzyliminio)-3-oxocyclohexa-1,4-dien-1-olate (molecule **2** of figure 17), of formula $C_6H_2(\cdots NHR)_2(\cdots O)_2$ where $R = n$-$CH_2C_6H_5$, adsorbed graphene, reproduced with permission from [120].

molecules and the graphene is also evidently very weak. Moreover, the weak interaction between the graphene and the the quinonoid zwitterion molecules indicates that the graphene is rather inert, which is also mentioned in other studies [49, 65].

The tetracyanoquinodimethane (TCNQH), i.e. $(NC)_2CC_6H_4C(CN)_2$, functionalized *p*-benzoquinonemonoimine zwitterion (6Z)-4-(butylamino)-6-(butyliminio)-3-oxocyclohexa-1,4-dien-1-olate (molecule **4** in figure 17), however, adopts a Stranski–Krastonov growth mode on the graphene, as indicated in figure 20. Unlike related quinonoid zwitterions, there seems to be little difference between the electronic structures of this TCNQH functionalized *p*-benzoquinonemonoimine zwitterion after it has been deposited on gold and graphene, for comparison.

4.2. The adsorption of molecules with carboxyl groups (COOH)

The presence of additional functional groups to derivatives of benzene molecules can significantly alter the magnitude of π–π interactions between the adsorbed molecules and graphene by giving rise to strong medium-range interactions involving π-orbitals of the substituent functional groups [74]. This has been studied thoroughly with the example of benzene, which has been systematically modified by increasing the number of

carboxyl groups (COOH) from 1 to 3, thus forming benzoic acid, isophthalic acid, and trimesic acid (figure 21 [74]). The carboxylic acid groups of molecules adsorbed on the graphene can electronically couple with nearby carbon atoms of the graphene, thus increasing the adsorbate–graphene interactions. Adsorbate attachment is expected to occur preferentially at structural defects in the graphene, such as the edges. Since the electronic structure of graphene is known to be sensitive to edges, such preferred adsorption would potentially change the optical gap through increasing of the width of the hole created in graphene by the carbonyl groups [118, 127]. The binding energy of the molecules to graphene, as compared to benzene, was greatly increased by the existence of carboxyl groups on the benzene ring (figure 22 [74]). The interaction between carboxyl groups and graphene is predicted to induce adsorbate dipoles through charge transfer between the molecules and graphene substrates. The computational results depicted in figure 22 show that the adsorption energy does not increase linearly with the number of COOH groups. This is thought to be due to the competing effects of π–π repulsion, which acts to decrease the adsorption energy, and the concomitant increase of the adsorption energy resulting from the increased number of COOH groups. In addition, with increasing number of COOH groups, the net charges transferred from the graphene to the adsorbate increase and so do the induced adsorbate dipoles [74]. As a result, the strength of adsorption increases, but as shown in figure 22.

An interesting application of molecules containing carboxylic acid is their use to cleave graphite into single layer
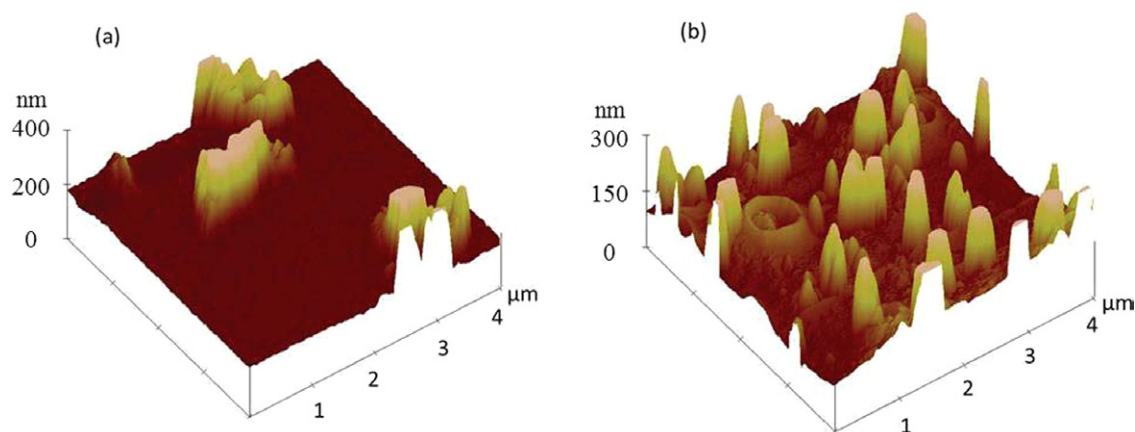
Figure 20. AFM images of the TCNQH = (NC)$_2$CC$_6$H$_4$CH(CN)$_2$)-functionalized (6Z)-4-(butylamino)-6-(butyliminio)-3-oxocyclohexa-1,4-dien-1-olate (molecule **4** of figure 17), i.e. C$_6$H$_2$($\cdots$NHR)$_2$($\cdots$O)$_2$ (where $R = n$-C$_4$H$_9$), thicker zwitterion films on (*a*) Au and (*b*) graphene, showing uneven wetting of the substrates. The roughness of (*a*) and (*b*) are about 200 nm and 150 nm separately. Adapted from [205], reproduced with permission of The Royal Society of Chemistry (RSC).
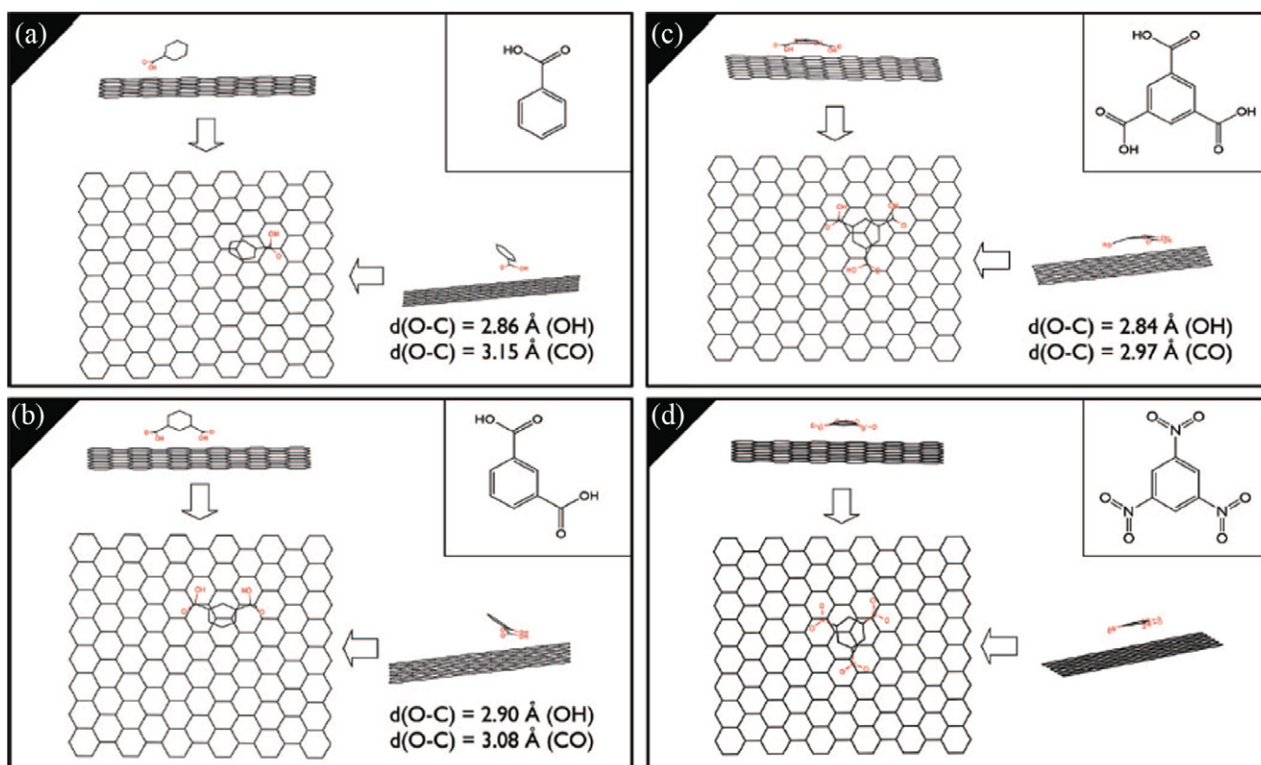
Figure 21. The adsorption of substituted derivatives of benzene on graphene: (*a*) BZA, (*b*) IPA, (*c*) TMA, and (*d*) TNB, reproduced with permission from [74], copyright (2009) American Chemical Society.

and multilayer sheets of graphene, as was demonstrated by An *et al* [76]. The use of 1-pyrenecarboxylic acid (PCA) with a nonpolar (hydrophobic) pyrene group and a polar (hydrophilic) carboxylic acid (COOH) group pointing out-of-plane can be instrumental for separating π–π stacked graphitic layers, as shown in figure 23. The COOH group of the PCA are key here; however, this demonstration is somewhat different from the main focus of this review in that the experiments were performed in a solution, and in that the molecules gradually penetrate the layered graphite rather than attaching to its surface. The nonpolar pyrene portion of PCA exhibits a fully

conjugated π-network very similar to graphene, so that PCA molecules are able to penetrate gradually into the graphite layers to form strong π–π stacking with the adjacent graphene layers. With the COOH group pointing out of the plane, as shown in figure 23, PCA places polar functional groups close to the graphene surface without disrupting the graphene's sp^2 hybridization. With the help of the polar medium water and agitation, functionalized graphene sheets are cleaved from the graphite [76]. Once cleaved, the graphene sheets remain functionalized by the PCA molecules, which allows stable dispersion in water.
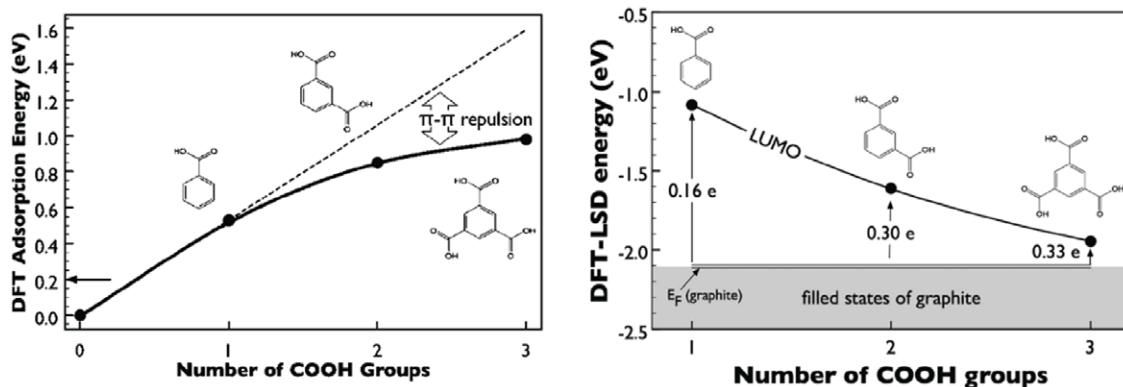
Figure 22. The adsorption energy increases with the increase number of COOH groups, while the LUMO energy shift closer to the Fermi level of graphene, reproduced with permission from [74], copyright (2009) American Chemical Society.
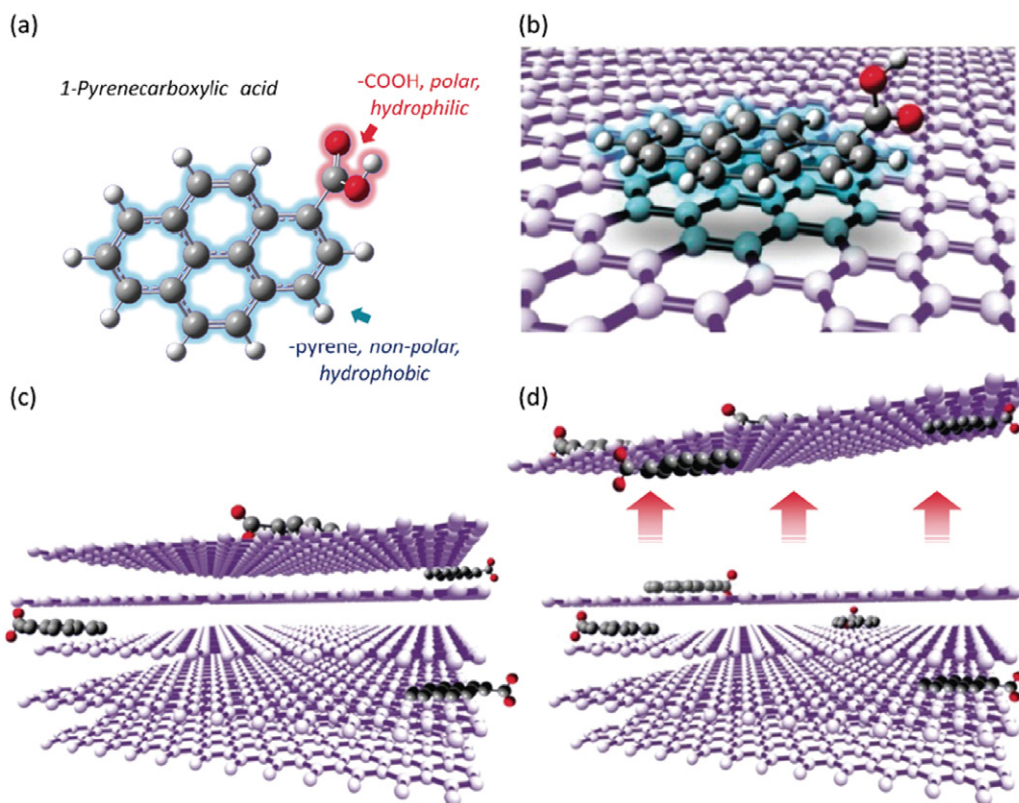
Figure 23. (*a*) Molecular structure of 1-pyrenecarboxylic acid (PCA) and (*b–d*) the interaction between PCA and graphene layers. From, reproduced with permission from [76], copyright (2010) American Chemical Society.

5. Other chemical modifications of graphene through molecular adsorption

The chemical modification of epitaxial graphene by the covalent attachment of nitrophenyl groups to the basal carbon atoms has been shown to be a successful route towards band gap engineering in graphene [75]. The adsorption results in the formation of covalent C–C bonds between the molecules and the graphene, thereby transforming the graphene carbon centers from sp^2 to sp^3 (figure 24) and introducing a band gap. Experimentally, there is indication of the formation of these new bonds in the characteristic broadening of the XPS C1s peak (figure 24(*b*)), which is attributed to sp^2 hybridized C atoms in the graphene. However, the peak broadening is also

thought to be due to *p*-type doping of graphene. Measurements of the sheet resistance of the epitaxial graphene revealed a characteristic increase of the sheet resistance upon covalent functionalization with the nitrophenyl groups, more than doubling the room temperature sheet resistance and creating a semiconductor-like temperature dependence of the sheet resistance (figure 24(*c*) [75]).

Graphene sheets can be functionalized across the entire surface, or selectively at the edges. The type of functionalization to some extent depends on the reactions used in the functionalization process [128, 129]. This has been shown for instance through 1,3-dipolar cycloaddition and amine-condensation reaction, through which dendron moieties with amino groups were selectively added to the center or the periphery of
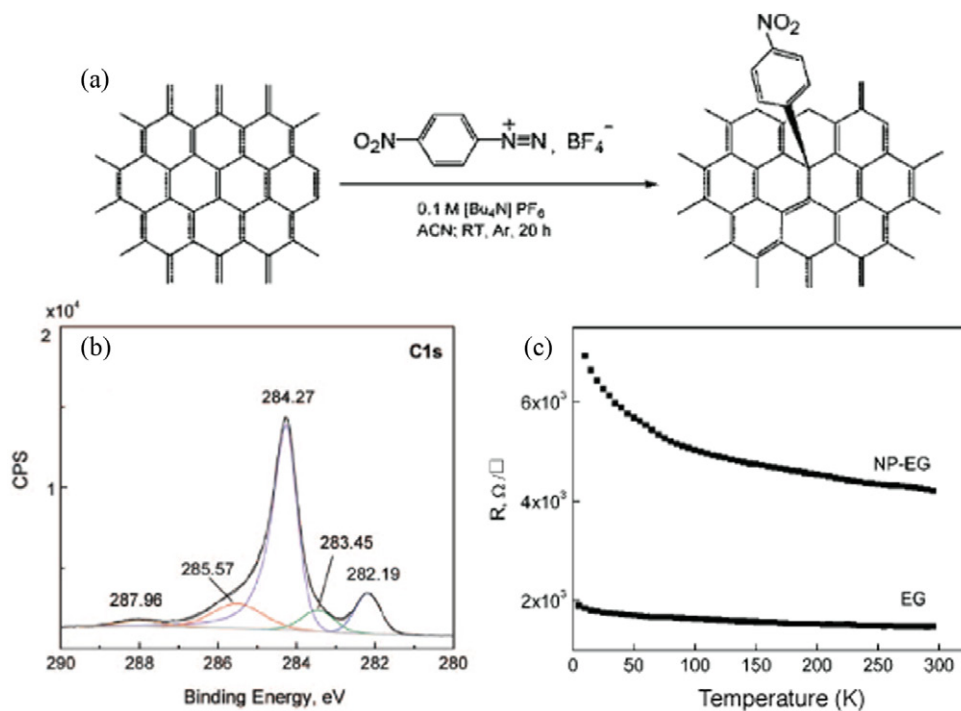
Figure 24. (*a*) Schematic of the spontaneous grafting of aryl groups to epitaxial graphene via reduction of 4-nitrophenyl diazonium (NPD) tetrafluoroborate; (*b*) XPS C1s core level sepectra of EG after functionalization with nitrophenyl; (*c*) temperature dependence of the sheet resistance of pristine graphene (EG) and nitrophenyl functionalized graphene (NP-EG) measured by the van der Pauw technique, reproduced with permission from [75], copyright (2009) American Chemical Society.

the graphene sheets [128]. Related to that, the reactivity of a single layer of graphene has been tested through the reaction of 4 nitrobenzene diazonium tetrafluoroborate and graphene, through which the graphene becomes functionalized with nitrobenzene. The reactivity was found to be larger for single graphene layers than for multilayers, and the graphene edges appeared to be more reactive than the interior of a graphene sheet [129]. Studies of aminotriazines molecular adsorption on graphene further suggest that the energy of adsorption increases linearly with the number of NH_2 groups added to the aromatic core [82]. This is because the NR_2 groups of a actually form bonds with the graphene [82].

The adsorption of 2,3-dichloro-5,6-dicyanobenzoquinone (DDQ), tetrathiafulvalene (TTF) and 1,1′ dibenzyl-4,4′-bipyridinium dichloride (BV2+) on graphene [79, 130] results in a geometry where the molecules tend to lie flat on the graphene layer, similar to benzene. Shin *et al* [130] suggested that the reduction potential of the molecules from graphene determines the interaction between graphene and the adsorbates. DDQ molecules with positive reduction potential act as acceptors and tend to induce *p*-type doping. This results in an increased work function of graphene. BV2+ molecules, with negative reduction potential, act as donors and cause *n*-type doping, thereby decreasing the work function of the graphene. It has been suggested that the larger reduction potential difference between adsorbed molecules and graphene results in a large amount of charge transfer [130]. It is further concluded that *p*-type doping has a negligible influence on the mobility of the graphene's charge carriers, while *n*-type doping usually significantly reduces the mobility of charge carriers in graphene [20, 130].

Extreme modification using a large moment molecular adsorbate, $TbPc_2$ (Pc = phthalocyananine), led to a magneto-resistive junction behavior [131], but the applicability to the graphene is unclear as is this example—the large magnetic moment adsorbate was placed on a graphene nano-constriction. Still these results suggest that some adsorbates might well induce a spin polarization and some magnetic anisotropy.

While this review has mostly focused on small adsorbates and larger but planar adsorbates, there is an abundance of studies addressing the adsorption of larger, 3D adsorbate molecules to achieve properties manipulation in the graphene layer. One of the outstanding examples to illustrate this point is the adsorption of fullerene molecules, C_{60}. Fullerenes are different from all other adsorbates considered in this study in that upon physisorption they form covalent bonds with the graphene. Theoretical studies conclude that fullerenes bind covalently to either the face of a graphene sheet or to the graphene edges [201–203]. On top of a graphene monolayer, the level of fusion of the fullerene with the graphene, that is, how many C–C bonds are formed between the two, is the determining factor for the electronic properties of the so-created 'nanobuds' [201]. The nanobuds are typically semimetallic if their cage opens up to fuse with the graphene. If the fullerene cage stays intact but binds covalently to the substrate, then also semiconducting properties are possible [201]. The periodic covalent attachment of fullerenes will preserve the Dirac cones of the graphene, but their position in the Brillouin zone can be effectively modulated by changing the fullerene's concentration [203]. Importantly, a band gap of approximately 0.35 eV can be opened by inducing randomness in the orientation of the fullerene adsorption [203].
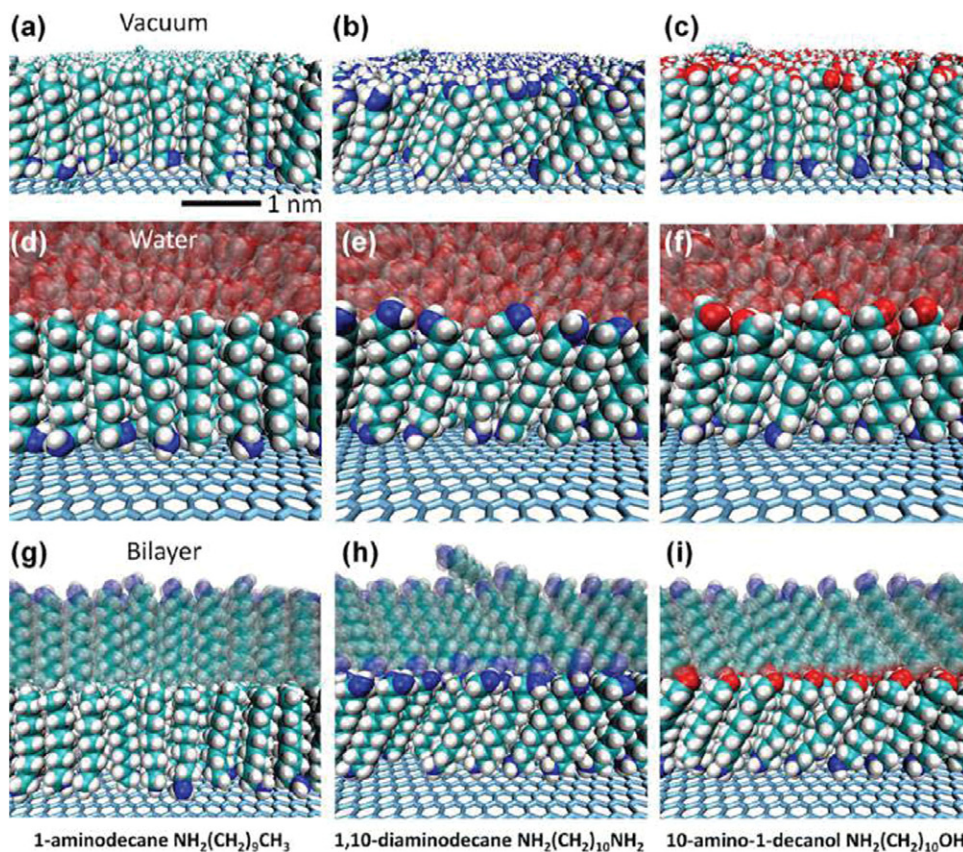
Figure 25. (Adapted with permission from [132], copyright (2013) American Chemical Society). Computed film structures on graphene. Each subpanel shows a perspective view of typical molecular packing arrangements in film structures formed following room-temperature molecular dynamics on a 13 nm × 15 nm graphene sheet. Methyl-, amine-, and methanol-terminated SAMs are shown in panels $a - c$, respectively. Water-solvated SAMs and molecule bilayer structures are shown in panels $d - f$ and $g - i$, respectively. These final structures were computed following 12 ns of SAM dynamics and an additional 4 ns to model the assembly of SAM/water interfaces or an additional 8 ns to model bilayer assembly via the adsorption of a second layer of molecules on the SAM.

Another exciting area is interfacing graphene and graphene derivatives with biological molecules [204]. Biological molecule adsorbates on graphene will be discussed in the following section.

6. The adsorption of biological molecules on graphene

One way to functionalize graphene is via the adsorption of biological molecules. In most cases this adsorption is achieved non-covalently, via the π–π interaction on the graphene plane. During the adsorption process the graphene may perturb or stabilize the native structure of these molecules, and in many cases also that of their self-assembled structures. A detailed mechanistic understanding of biological-molecule-graphene interaction is thus not only important for nanoscale materials design but also because it may shed some light on critical mechanisms such as protein folding, misfolding, and aggregation—information that is not readily available. This biomimetic approach may also exploit the molecular recognition property of peptides for which an accurate knowledge of the peptide structure is necessary. While a number of experimental groups have visualized the binding properties of peptides on the graphene using techniques such as AFM and STM,

information on the geometric structure and the nature of the bio-molecule-graphene interaction could only be obtained by supplementing the experimental data by theoretical modeling and simulation. In this regard, classical molecular dynamics (MD) simulations employing semi-empirical interaction potentials have been most popular, although recent efforts have also turned to the more accurate, albeit computationally demanding, methods that stem from density functional theory, as we shall see. While it is not possible to document every study in this review, a short summary of some the recent work in the area is provided below.

Atomic-scale molecular dynamics simulations of alkylamine self-assembled monolayer (SAM) films on graphene [132] show that the SAM architecture can be tailored for use in emerging applications (e.g. electrically stimulated nerve fiber growth via the targeted binding of specific cell surface peptide sequences on the functionalized graphene scaffold). These simulations quantify the changes in film physisorption on graphene and the alkyl chain packing efficiency by making the film surface more polar and by changing the terminal groups from methyl to amine to hydroxyl. The typical stacking of three different molecules on graphene is shown in figure 25. One finding is that the mode of molecule packing dictates the orientation and spacing between terminal groups on the surface of the SAM, which in turn determines whether

Table 2. Computed Protein − SAM Adsorption Energies on SAM-Functionalized Graphene (energies in kcal mol^{-1}). Adsorption energies were estimated from HFB − SAM van der Waals and electrostatic interaction energies. Error estimates are in parentheses and were averaged over 300 structures, sampling every 10 ps during the final 3 ns of dynamics. Adopted with permission from [132], copyright (2013) American Chemical Society.

Protein-SAM adsorption	Terminal group	Electrostatic	van der Waals	Total
orientation (a)	−CH$_3$	−4.3 (2.4)	−24.5 (4.6)	−28.8 (6.2)
	−CH$_2$NH$_2$	−12.3 (9.8)	−12.3 (3.8)	−24.6 (11.7)
orientation (b)	−CH$_3$	−4.5 (2.4)	−30.2 (5.5)	−34.8 (7.2)
	−CH$_2$NH$_2$	−37.3 (19.7)	−12.2 (3.9)	−49.6 (20.0)
orientation (c)	−CH$_3$	−4.7 (1.5)	−42.3 (5.3)	−46.9 (5.9)
	−CH$_2$NH$_2$	−3.5 (7.0)	−11.3 (3.1)	−14.8 (7.6)
orientation (d)	−CH$_3$	−1.2 (1.9)	−27.2 (4.8)	−28.4 (5.3)
	−CH$_2$NH$_2$	−9.2 (9.3)	−11.8 (4.7)	−20.9 (10.2)

the successive layers build up via the formation of bilayers of the molecule or through the immobilization of other molecules. These simulations show the formation of ordered, stable assemblies of monolayers and bilayers of decylamine-based molecules on graphene. The simulations also indicate that the alkyl chain must be sufficiently long, and the surface concentration of molecules sufficiently high, to direct the formation of ordered, tightly packed upright SAMs, as opposed to molecules physisorbed lengthways, on the graphene. The evaluated relative contributions of electrostatic and vdW interactions shown in table 2 show the dominant role of the latter for methyl termination for all orientations. The differences found for the relative role of these two interactions for amine termination are interesting and understandable.

Further advancement in understanding the nature of the bonding of peptides on graphene sheets was obtained from STM images taken in an ultra-high vacuum, as well as, under ambient conditions [133], of two synthetic model peptides R$_4$G$_4$H$_8$ and F$_4$G$_4$H$_8$, containing four kinds of residue groups (Phe-benzyl, Arg-carbamidine, Gly-hydrogen, and His-imidazole). An examination of the conformational dynamics of these peptide assemblies adsorbed on a graphene sheet in water at 300 K, using molecular dynamic simulations [133], showed that both peptide assemblies are mostly in the β-sheet structure, and that the interaction energy of the four different residues with graphite surfaces follows the order of Phe > His > Arg > Gly, consistent with their brightness contrasts in STM images. The correlation between the brightness contrasts with the peptide sequence and the related interaction energy may shed light on the sequence and conformation effects on the peptide assemblies.

Akdim *et al* [134] used a combination of classical molecular dynamics simulations and density functional theory calculations to explain their experimentally observed doping behavior of single-layer graphene upon adsorption of peptides HSSYWYAFNNKT (P1) and HSSAAAAFNNKT (P1-3A) in field-effect transistors (GFETs). They concluded that the observed *p*-doping by the adsorbed P1 peptide may have arisen from an intrinsic doping mechanism. The charge transfer and electron transport calculations, based on the lowest energy structure of the hybrid material system, suggested that the $\pi - \pi$ stacking of the aromatic residues and proximate backbone on the graphene surface in P1 may have had a role in the *p*-doping. They trace the observed change from *p*- to *n*-doping on substitution of three of the aromatic amino acid residues to Ala in P1 − 3A to altered charge transfer characteristics.

In a related work, Katoch *et al* [135] performed AFM, Raman, and Fourier transform infrared (FTIR) spectroscopy to examine the structure of peptides bound to graphene and graphite. The AFM images (see figures 26(*a*) and (*b*)) of the graphene before and after incubation with the peptide, together with the infrared spectrum shown in figure 27 led to the conclusion that the peptides bind noncovalently to the graphene and HOPG and form secondary structures both in powder form and in an aqueous medium. The dominant structure in the powder form is an α-helix, which undergoes a transition to a distorted helical structure in an aqueous solution. AFM images indicate that identical adsorbed layers are formed upon incubation on the graphene and HOPG. The Raman spectra of the system further corroborates that the functionalization of the graphene is achieved non-covalently since the incubation does not cause any chemical perturbation to the graphene. The results of this multiprobe experiment not only provided useful information on the striking features of adsorbed peptides, it also validated earlier conclusions of similar systems which were derived only on the basis of MD simulations [136]. Since MD simulations can be performed relatively easily, these results demonstrate that MD simulations can be relevant for predicting the behavior of peptide-functional groups on graphene and identifying proper functional groups for various analytes.

Ou *et al* performed MD simulations of the adsorption, conformational dynamics, and dimerization of two chains of a de novo designed the α-helical peptide on a graphene sheet in explicit solvent at 310 and 330 K [137] to find that the two chains were mostly dimeric and keep α-helical structure in solution, whereas they unfolded and assembled into an amorphous dimer on the graphene surface. The C-terminal residue (see table 3) showed a preference to adsorb on the graphene surface because of the strong interactions of the Arg13, Ile14, and Lys15 residues with the carbon atoms, leading to a fast unfolding of the α-helix starting from the C-terminal region. The β-sheet conformation was not observed in all MD runs within the 15–200 ns times scale, which indicated that the α-helix to β-sheet transition for this short peptide at the graphite surface was a slow process, similar to the slow transition dynamics of globular protein reported experimentally. These simulations were able to identify the regions of strong interaction between the peptide (residues Arg13-Ile14-Lys15) and the graphene and trace the initiation of the α-helix unfolding of the peptide at the graphene surface to this region.

As with most single-layered materials, the nature of the binding between atoms on a plane is different from that at
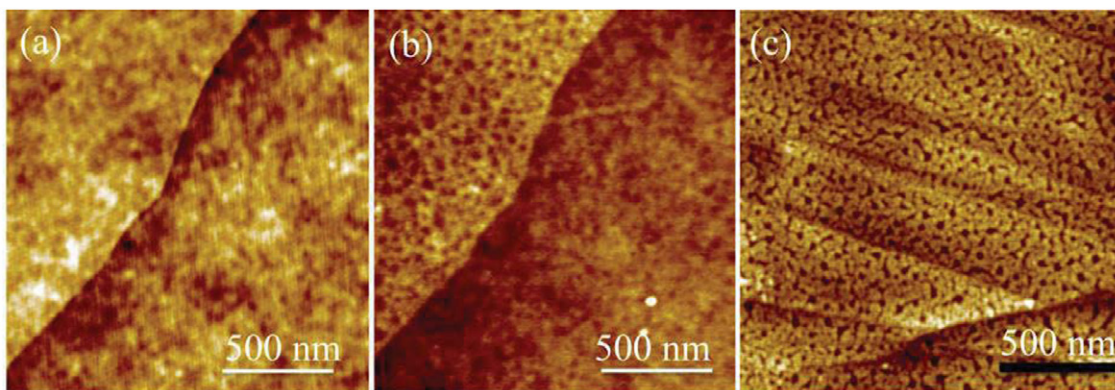
Figure 26. (Adapted with permission from [135], copyright (2012) American Chemical Society). AFM topographic image of graphene (*a*) before and (*b*) after incubation with the peptide. (*c*) Topographic AFM image of HOPG incubated with the peptide.
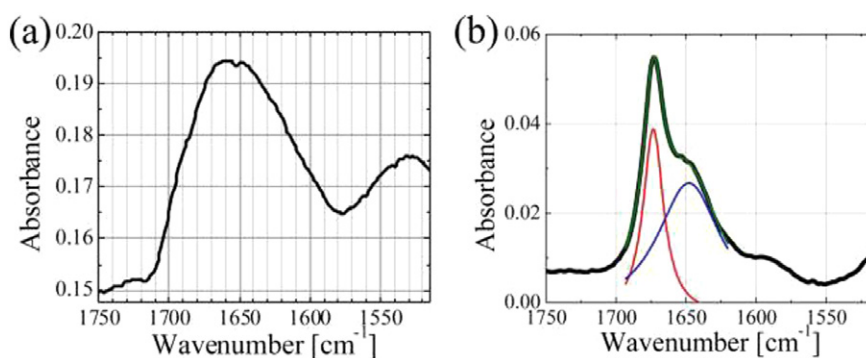
Figure 27. (Adapted with permission from [135], copyright (2012) American Chemical Society). (*a*) Infrared spectrum of GBP in powder form, showing both amide I and amide II bands. (*b*) Infrared spectrum of GBP in D2O, showing the amide I band. Red and blue curves are obtained by fitting two Lorentzian functions to the experimental data. The peaks are located at 1673 and 1648 cm^{-1}. The green curve is the result of some of these functions.

Table 3. (Adopted from [137]). Set-up details of all the MD simulations and the Cα-rmsd of the peptide at the end of each MD run. The two peptide chains are labeled as P1 and P2, with the C-terminus being denoted by letter C. The carbon atoms of the graphene sheet are in yellow. To mimic the experimental neutral pH condition, the side chains of the Asp, Glu, Arg, and Lys are charged (Asp $-$, Glu $-$, Arg $+$, Lys+).

System	Name of MD run	T	Number of atoms	Time (ns)	Initial state	rmsd of P1 (nm)	rmsd of P2 (nm)
Pep	A1	310 K	12906	60		0.20	0.06
	A2	310 K	12906	60		0.07	0.08
Pep + Gra	B1	310 K	12474	15		0.31	0.33
	B2	310 K	12474	15		0.38	0.18
	B3	310 K	12474	60		0.27	0.09
	B4	310 K	12474	60		0.24	0.33
	B6	330 K	12474	200		0.41	0.18
	B7	330 K	12474	200		0.29	0.34
	B5	310 K	12483	200		0.21	0.33
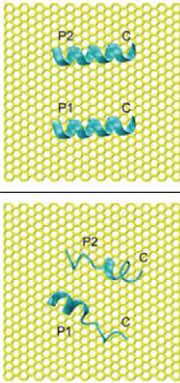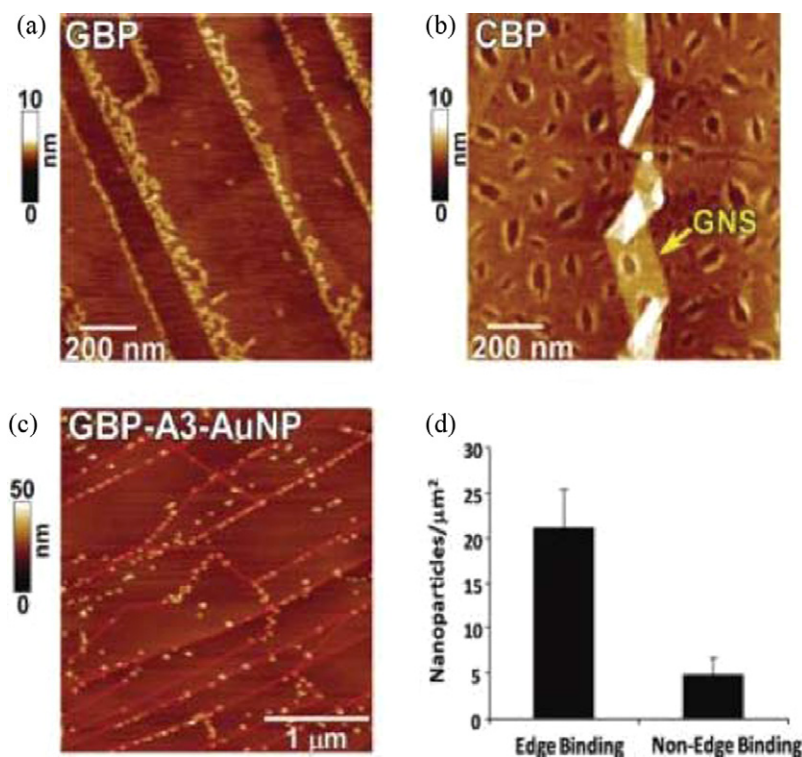
Figure 28. AFM topographic images obtained from thr graphene surface exposed to (*a*) GBP peptide and (*b*) CBP peptide, which assembled onto the graphene edges and plane, respectively. A graphene nanostrip (GNS) is indicated by the arrow. (*c*) AFM topographic image obtained from a graphene surface exposed to AuNPs functionalized with the GBPA3 peptide (GBP-A3-AuNP), which assembled onto the graphene edge. Graphene edges (red lines) identified from sub-10 nm AFM height images are depicted for clarity. (*d*) Bar chart showing the number of GBP-A3 peptide-functionalized nanoparticles binding to the edge and nonedge regions of graphene.

the edges. For graphene, the sp^2-hybridized C–C bonds on the plane are replaced by the relatively weak dangling =C-C (H)-C= bonds at the edges, which are suitable for covalent functionalization. The ability to functionalize graphene in two ways—non-covalently on the plane and covalently at the edges—was exploited by Kim *et al* [136] in a combined experimental and computational study of several types of graphene binding peptides, identified from a combinatorial phage display peptide library. These peptides were found to bind to the planar surface of the graphene via π–π stacking and to the edges via electrostatic interactions. Interestingly, Kim *et al* [136] designed a bifunctional peptide (A3—EPLQLKMGGGG) from graphene—and gold-binding peptides, which they used to direct the assembly of gold nanoparticles to the graphene edges (see figure 28). Their AFM analysis confirmed that the peptide indeed assembled at the grapheme edges. Furthermore, their electronic measurements using mechanically ablated graphene field-effect transistors showed that the edge—and plane binding peptides, both affected the electronic properties of the graphene, a finding with technological implications. On the other hand, the dodecameric carbon nanotube-binding peptide (CBP) with the sequence HSSYWYAFNNKT7 was found to decorate the HOPG surface uniformly (see figure 28(*b*)) forming a monolayer with distinct pores on the planar HOPG surface. Their comparative study of the binding of GBP and CBP on the graphene showed that the GBP assembles preferentially at the graphene edges and also that the binding of the GBP to the edge affects the electronic structure of the graphene more than when the CBP binds to the planar graphene surface.

The graphene interacts strongly with the hydrophobic components of biomolecules, potentially altering their conformation and disrupting their biological activity. Alava *et al* [138] immobilized the protein Concanavalin A onto a self-assembled monolayer of multivalent tripodal molecules on a single-layer of the graphene, using a quartz crystal microbalance (QCM) to show that this biomolecule retains its affinity for polysaccharides containing α-D-glucopyrannosyl groups as well as for the α-Dmannopyranosyl groups located on the cell wall of Bacillus subtilis. QCM measurements on unfunctionalized graphene indicate that the adsorption of Concanavalin A onto the graphene is accompanied by a near-complete loss of these functions, suggesting that interactions with the graphene surface induce deleterious structural changes to the protein. Given that Concanavalin A's tertiary structure is thought to be relatively robust, these results suggest that other proteins might also be denatured upon adsorption onto the graphene, such that the graphene-biomolecule interface must be considered carefully. Multivalent tripodal binding groups address this challenge by anchoring proteins without loss of function and without disrupting the graphene's desirable electronic structure.

The π − stacking interactions on the graphene plane also provide the opportunity for DNA sequencing and recognition, as has been proposed by Min *et al* [139, 140]. For the proposed fast sequencing, the binding energy needs to be strong enough to hold nucleobases on the graphene and reduce noise in measurement, as well as being weak enough to translocate a single-stranded DNA over a graphene nanoribbon in a nanochannel. While these applications are important in themselves,
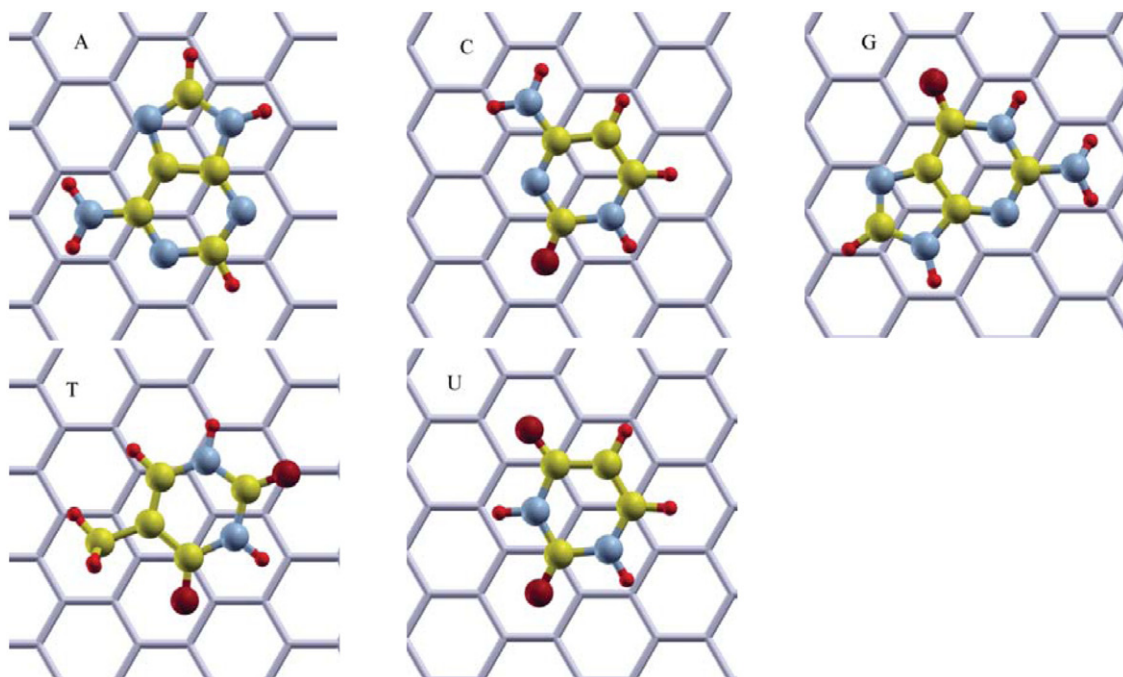
Figure 29. Optimized orientation of adenine (A), cytosine (C), guanine (G), thymine (T), and uracil (U) on graphene.

they also provide opportunities for testing some of the recent advances that have been made in incorporating van der Waals (vdW) interactions into DFT. Several theoretical studies on the interaction between nucleobases and graphene have thus been reported. Using DFT-LDA, Gowtham *et al* [141] showed that all the nucleobases are separated from a graphene sheet by about 3.5Å and the binding is strongest for guanine (14 kcal mol^{-1}), while it is similar for other nucleobases (11 kcal mol^{-1}). They also showed that translocation parallel to the graphene surface has a low barrier, maximally 2.3 kcal mol^{-1}. Antony *et al* [142] applied B97-D functional to optimize the same systems to find significantly closer base − graphene distances of about 3.0Å. Another recent study by Berland *et al* [143] using Dion's non-local functional [144] predicts, for an adenine molecule, the adsorption energy of 16.4 kcal mol^{-1} at an equilibrium separation of 3.5Å. This was followed by the work of Le *et al* who applied a set of DFT based techniques to examine the trends in the binding energies and adsorption heights of the nucleobases on the graphene [145], summarized in table 4. In a more recent study [146], symmetry-adapted perturbation theory [147], with input from several other DFT based methods was used to further analyze these binding characteristics.

Since a number of DFT based computational techniques [144, 148–150] have been proposed to account for the contribution of van der Waals interaction to the binding of molecules on surfaces such as graphene, two recent studies [145, 146] provide an analysis of the computational cost associated with each method as well as the differences in the binding energy and binding distance of DNA fragments on graphene.

Figure 29 illustrates the optimized structures of the nucleobases on the graphene. According to Le *et al* while there are some disagreements in the results from the application of the different techniques in predicting binding energies, there is good agreement in their prediction of the strength of the
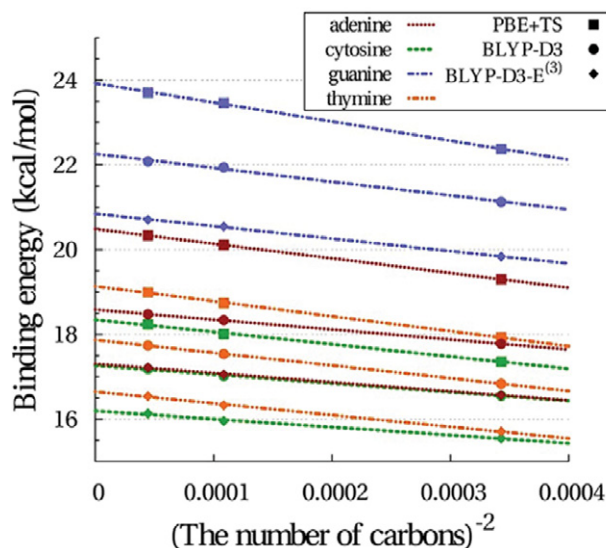
Figure 30. (Adapted with permission from [146], copyright (2013) American Chemical Society). Binding energies with increasing flake sizes to obtain the extrapolated values for the infinite sizes. The binding energies are plotted against $1/N$, where N is the number of carbon atoms in the flake.

interactions of the nucleobases on the graphene which follows the order Guanine > Adenine > Thymine > Cytocine > Uracil. Cho *et al* [146] further examined the binding energies of flakes of increasing size of four nucleobases on the graphene to find that they lie between $18 − 24$ kcal mol^{-1} (see figure 30). These values are, however, twice as large as what they found for the same set of nucleobases on naphthalene. Since screening effects are not included in these calculations, some questions still remain about their reliability. Non-covalent interaction of DNA bases with graphene provide another avenue for understanding the subtleties in these interactions.
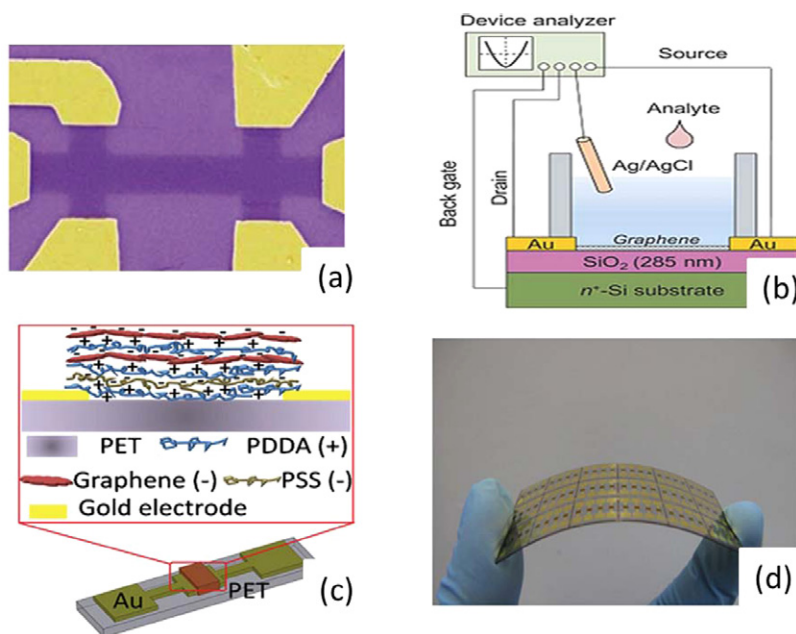
Figure 31. Graphene based sensors: (*a*) gas sensor, reproduced with permission from [30]; (*b*) chemical molecules sensor, reproduced with permission from [119], copyright (2011) American Chemical Society; (*c*) and (*d*) cancer sensor on a flexible PET substrate, reproduced with permission from [154], copyright (2011) AIP Publishing LLC.

7. Graphene sensor devices

Due to very large changes in the relative conductivity that are possible as a result of the charge doping that occurs within the graphene due to the charge transfer with a number of adsorbates, together with its uniquely high surface-to-volume ratio, graphene has been touted as enabling or improving a variety of gas sensors, chemical sensors, and biosensor applications. A number of device concepts have been investigated [30, 151–153], applying graphene as the sensing element for gasses and biomolecules. As such, those devices expand upon the success of the structurally similar carbon nanotubes (CNT), which are currently applied in various sensors [154–157]. The electronic properties of graphene translates into low intrinsic noise in the device signal, in spite of the low carrier concentration, and thus superior sensitivity. Even a few electrons transfered to or from the graphene sheet can cause notable changes in the carrier concentration in graphene [30], which may not be large in an absolute sense are huge in a relative sense, as noted in the introduction. Moreover, the graphene-based sensors allow four-probe measurements, which further improves the device accuracy. Examples of graphene-based sensor concepts are shown in figure 31.

The fundamental concept is that molecular adsorption on the graphene modifies the charge carrier concentration near the Dirac point, resulting in the characteristic *p*-type or *n*-type doping of the graphene, as has been the main focus of this article. We reiterate that the doping level, and with it the change in sign and magnitude of the conductivity of the graphene, depends on the amount of adsorbed molecules and their efficiency as electron acceptors and donors. As such, graphene-based sensors are found to be partially chemically selective if the magnitude *and* sign of the sensing signal (i.e. the sheet conductivity) is evaluated in a device, as seen in figure 32. More
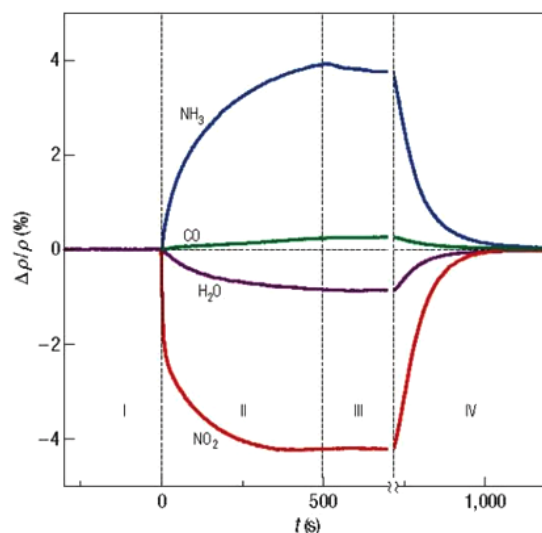
Figure 32. The sensitivity of graphene to the chemical doping. The changes of the resistivity induced by the adsorption (II) and desorption (IV) at 150°C of four different small gas molecules, reproduced with permission from [30], demonstrating the chemical selecivity of the sensor device.

advanced devices evaluate the change in the majority of carrier concentration in transistor or Hall bar device structures more directly, again as seen in figure 32 [30]. In a Hall bar structure, the sensitivity changes linearly with the concentration and type of adsorbed molecules, as the adsorbate species directly modify the type of majority carriers as well as the charge carrier density. Both determines the experimentally accessible Hall conductivity, which is defined as $\sigma_{xy} = 1/\rho = ne/B$. Here, n represents the charge carrier concentration, where the sign of the conductivity corresponds to the type of carriers, electrons (−) or holes (+). The e is the elementary charge, and B is the applied magnetic field. A similar concept
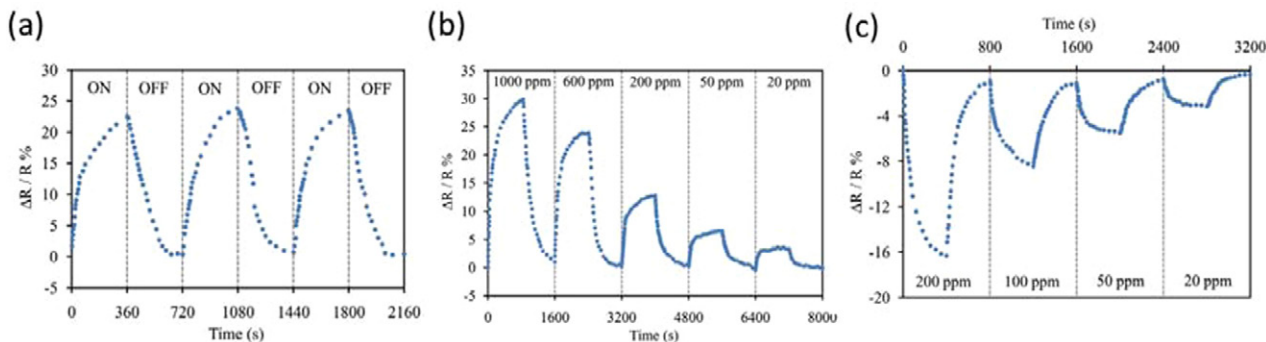
Figure 33. Reversibility and sensitivity of a graphene-based gas sensor as function of time for the detection of 1000 ppm of NH_3 using Joule heating during the desorption step. (*a*) With Joule heating during the desorption step, the sensor exhibits fully reversible response. (*b*) Sensor response to varied NH_3 gas concentrations in air, with Joule heating during desorption. (*c*) Sensor response for different concentrations of NO_2 in air. The change of normalized resistance corresponding to different concentration of NH_3 (*b*) and NO_2 (*c*) in air, reproduced with permission from [158].
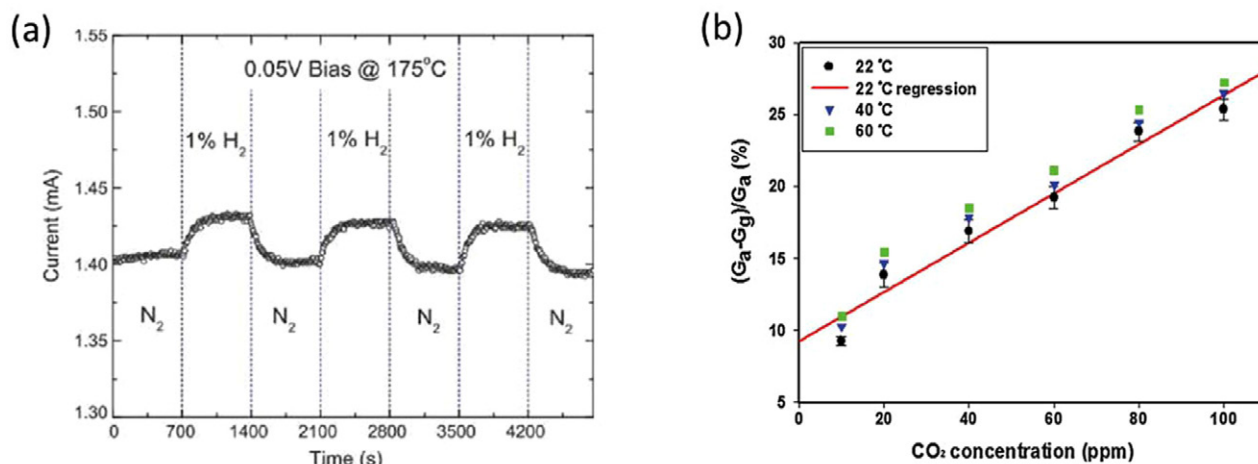
Figure 34. (*a*) Resistance response to 1% H_2 at a 0.05 V constant bias, reproduced with permission from [165], (*b*) Conductance changes at different concentrations of CO_2, reproduced with permission from [167].

applies in transistor structures, where the transistor base is graphene based. The source–drain resistance is now evaluated as a function of charge carrier concentration in the graphene base, which again can be sensitive to adsorbed gas molecules. Generally, all graphene-based sensors are based on the detection of changes in the electronic conductivity of the graphene caused by adsorbates [30, 157].

The adsorption of molecules with relevance for industrial, environmental, and medical applications for graphene was studied in depth. Often, graphene-based sensors for NO_2 and NH_3 were fabricated both on Si/SiO$_2$ as well as on SiC substrates [13, 15, 16, 158–164]. It has been suggested that the performance of a sensor built on SiC has distinctive advantages over SiO$_2$-based sensors, such as higher electrical conductance and lower intrinsic noise. When exposed to NH_3 molecules, the carbon–nitrogen bond is easier to form at the edges of the graphene [13], and a maximum response to the adsorption of NH_3 was found for multiple-layer graphene samples with 2 nm thickness [16]. Improvements of graphene-based sensors for NH_3 were achieved by Yavari *et al* [158] by creating a graphene-based foam-like porous 3D network for gas adsorption, coupled with Joule heating for thermally activated gas desorption. The sensors were found to exhibit increased sensitivity, excellent reliability, are

in principle low-cost and can be fully recovered by Joule-heating (figure 33).

The sensitivity of graphene to other gaseous adsorbates can be engineered by chemical modification of the graphene surface. For example, detectors for H_2 were achieved by covering epitaxial graphene on SiC substrates with a thin layer of Pt as catalyst [165, 166]. While H_2 molecular adsorption on the graphene by itself is hindered, as discussed in section 2, the adsorption of atomic hydrogen can be significant. The Pt aids in the dissociation of molecular hydrogen, so that the sensitivity of the graphene to H atoms can be exploited. Once dissociated, the atomic hydrogen diffuses to the interface between Pt and the graphene with a concomitant increase of the electrical conductance. Figure 34(*a*) shows a characteristic decrease of the electrical resistance in response to exposure to 1% H_2 [165].

CO_2 sensors were fabricated by mechanically cleaving flakes of highly oriented pyrolytic graphite (HOPG), followed by lithographic patterning, liftoff and fabricating electric contacts [167]. The so-achieved CO_2 sensor works under ambient conditions and at room temperature. Compared to conventional sensors it has a faster response time (less than 10 s) and a short recovery time because of the weak interaction between CO_2 and the graphene. The conductance of the sensor shows significant changes when exposed to CO_2 gas in the air and linearly
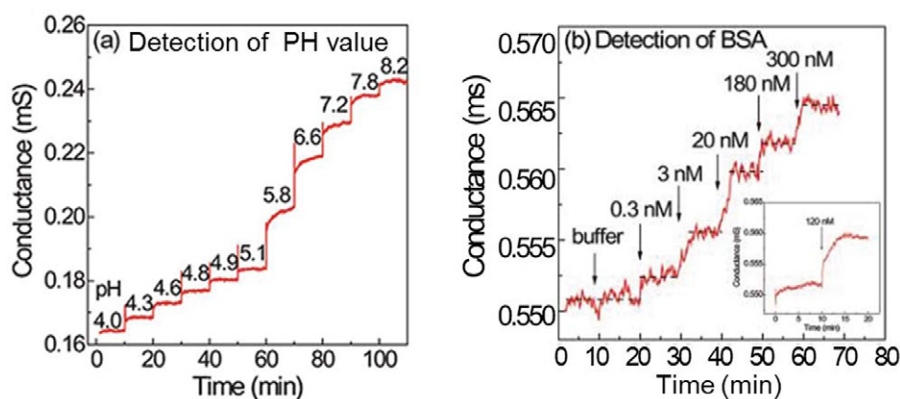
Figure 35. Detection of the pH value and biomolecule (Bovine serum albumin (BSA)) by graphene based sensors, reproduced with permission from [157], copyright (2009) American Chemical Society.

Table 4. Binding energies (meV) of nucleobases on graphene and optimized nucleobase-graphene separations (Å, in parentheses). Taken from [145].

Nucleobase	DFT-D				vdW-DF		vdW-DF2	
	sTS	TS	DFT-D2	DFT-D3	nsc	sc	nsc	sc
A	829 (3.29)	849 (3.28)	636 (3.18)	618 (3.38)	637 (3.50)	634 (3.50)	594 (3.37)	588 (3.39)
C	724 (3.32)	745 (3.31)	573 (3.20)	567 (3.38)	582 (3.50)	579 (3.51)	546 (3.38)	540 (3.41)
G	959 (3.26)	986 (3.25)	770 (3.13)	733 (3.33)	750 (3.45)	742 (3.45)	717 (3.33)	699 (3.35)
T	742 (3.35)	763 (3.34)	583 (3.22)	570 (3.42)	607 (3.53)	603 (3.53)	558 (3.41)	545 (3.43)
U	664 (3.31)	682 (3.30)	515 (3.20)	512 (3.38)	543 (3.49)	539 (3.49)	501 (3.37)	496 (3.39)

proportional to the concentration of CO_2 gas as it increased from 10–100 ppm, as shown in figure 34(*b*).

While any gas molecule that alters the charge carrier concentration in the graphene upon adsorption can also be detected by a graphene-based sensor, chemical selectivity is rarely ensured. Notably, sensors for O_2 sensors were easily built from graphene on Cu foil [164]. Such sensors exploit that O_2 molecules act as a *p*-type dopants as described above. Sensors for the toxic gas H_2S, made from ZnO-chemically converted graphene films, exhibited outstanding sensitivity to very low levels (2 ppm) of H_2S in oxygen at room temperature [168]. The graphene based humidity sensor exploits the sensitivity of the graphene's conductance to H_2O [169] (see section 2.2 above). Other graphene-based sensors for NO, CO and Cl_2 sensors are also worth noting [170–172].

It has even been suggested that graphene based sensors have the potential to detect biomolecules from the environment, to potentially detect various environmental contaminants and diseases. One example is the sensor for pH values and biomolecules, as shown in figure 35(*a*). As has been indicated, the Dirac points of the graphene shift reversibly upward with increasing pH [157, 173]. The sensitivity of graphene-based sensors to a variety of biomolecules, including glucose, protein and cancer cells [154, 157, 174] has been demonstrated. A flexible, low-cost and label-free graphene based cancer marker biosensor (figures 31(*c*) and (*d*)) was able to detect an extremely low concentration of cancer cells in a large detection range, exhibiting improved sensitivity as compared to the current widely used cancer marker biosensors [154]. Notably, it has been shown that the performance of the graphene sensor devices can be enhanced in an aqueous solution: graphene field effect transistors (Gra-FETs) suspended in aqueous solutions [173] showed an improved signal-to-noise ratio

by 14 dB in the frequency regime below 1 kHz for both hole and electron carriers as compared to those supported by SiO_2 substrates. An interesting trend is that some graphene based sensors are able to detect both the changes of resistance and mass of the graphene upon adsorption [155]. This approach, if improved further, has the potential to further increase sensitivity and perhaps chemical selectivity.

In reviewing the studies of molecule adsorption on graphene, it is evident that graphene as a gas sensor is problematic, even with very well defined graphene. It is certainly true that adsorbates can change the relative conductivity significantly, but so many adsorbates do this, that separating one adsorbate out from other ambient effects is difficult. How does one distinguish one adsorbate from another without functionalizing the graphene itself for some chemical specificity? If the doping of the graphene is competing with the band gap effects, huge variations in relative conductivity are possible— both increases and decreases in conductivity that then depend not only on the adsorbate but adsorbate coverage.

8. Conclusion

The modification of the electronic structure of graphene though simple molecular adsorption is clearly possible, and the impact of the organic adsorbates reviewed in this article on the band structure of the graphene is summarized in table 5. The resulting changes to the graphene electronic structure are highly dependent on the competition between intermolecular interactions and lateral variations in the molecule—substrate interactions, as well as the adsorbate graphene substrate interactions. The adsorbate–graphene substrate interactions can

Table 5. Summary of the changes in band structure and doping type in graphene with the adsorption of the molecules reviewed in this article.

Molecule type		Type of doping achieved	Gap created	Fermi level in the gap[a]	References
Small gas molecule	NO_2	*p*-type	Yes	No	[11, 12, 194, 195]
	H_2O	*p*-type	Yes	No	[11, 12, 50, 55, 69, 196]
	O_2	*p*-type	Yes[b]	No	[13–15, 197, 198]
	NH_3	*n*-type	Yes	No	[11–16, 55, 68, 199]
	CO, NO	weak *n*-type	No[c]	—	[11, 12]
	N_2O_4, weak donor	Nothing	No	—	[52, 53]
	H2, donor	*n*-type	Yes	Yes	[19, 59, 106, 200]
Planar molecules	Benzene and naphthalene	Nothing	No	—	[74, 80–82]
	Benzene and naphthalene with NH2 groups	*n*-type	Yes	No	[71, 82, 118, 127]
	TPA and An-Br	*p*-type	—	—	[71]
	An-CH3	*n*-type	—	—	[71]
	Diazonium salts	*p*-type	Yes	No	[89–92]
	TCNQ, F4-TCNQ and TCNE	*p*-type	Yes	Yes	[53, 70, 78, 108–110]
	PTCDA	*p*-type	No	—	[112–115]
	VOPc	*n*-type	—	—	[109]
	2,4′ BTP	—	No	—	[119]
Planar molecules with large intrinsic dipoles	Zwitterions	—	No	—	[120]
	Benzene with COOH groups	*n*-type	Yes	No	[74, 118, 127]
Covalently bonded 3D molecules	Fullerenes	—	Yes	Yes	[201–203]

[a] The position of E_F is based on the initial doping and type of graphene investigated and not necessarily representative of free standing pristine graphene. The position of the chemical potential may also be affected by the concentration of adsorbed molecules. This latter complication is evident in the adsorption of NO_2 [1], H_2 [106], F4-TCNQ [70, 98, 109] and diazonium salts [89–92] studies, so that E_F could lie within the band gap, but depending on the amount of adsorbed molecules.
[b] The type of graphene substrate makes a difference in E_F and the band gap opening. For instance, the adsorption of O_2 in single layer graphene and bilayer graphene are different [197, figure 2].
[c] Although the interaction is very weak, the adsorption of CO may induce a band gap opening in the nanoscale graphene [55].

occur in a mutiplicity of ways, both by breaking the local graphene symmetry from C_{6v} to C_{3v} or less and through charge transfer to the graphene. Adsorbates may dope the graphene either *p*-type or *n*-type depending upon the reduction potential. Yet, the interaction also depends on the structure of the graphene: it is generally much easier for molecules adsorbed on doped graphene and graphene with defects.

Yet the multitude of molecular adsorption studies are very useful in understanding the influence of the environment on graphene and pave the way for a better graphene-based device design. For instance, the successful control of the extrinsic doping level through substrate or adsorbate interactions could facilitate the microfabrication of graphene-based *p–n* junctions.

Opening a band gap in graphene fundamentally means lowering the C_{6v} point group symmetry to something less symmetric (C_{3v}, C_{1h}, etc), so that the conduction band and valence band are no longer degenerate at the Dirac point in charge neutral graphene. This is the fundamental concept behind the various widely publicized approaches to engineering a band gap in graphene, such as strain engineering [175–178], spatial restriction, for example via graphene nanoribbon fabrication [179–188], controlling the density of electrons as in adsorbate hybridization [16–21, 55, 64, 89, 189]. All these approaches to opening a band gap in graphene have major flaws when the goal is the retention of the unique properties of graphene while opening a band gap. The effective mass for uniaxially strained graphene, which is really the key parameter, in addition to the band gap, is a major problem as the increase in effective mass is usually considerable [178]. For graphene nanoribbons the situation is worse. The huge increase in

effective mass that may be inferred from many of the band structure calculations of graphene nanoribbons is complicated by significant edge scattering. This leaves adsorbate or substrate induced band gaps as a more promising avenue for the band gap engineering of the graphene. Substrate interactions are very hard to control. For example, a band gap of 0.26 eV has been experimentally determined for graphene on SiC [10], but is controversial and is in any case not a true band gap as the graphene is heavily *n*-type doped and the chemical potential (Fermi level) does not fall in the gap. The application of a perpendicular electric field should open a band gap up to 0.25 eV in the graphene heterolayer structures and renders the transport insulating [190–193]. But overall, efforts at opening a band gap without large decreases in carrier mobility by seeking a better adsorbate to control the band gap of the graphene seem more promising as long as, again, ambient effects can be diminished and made negligible.

Acknowledgements

Jie Xiao, Jing Liu, Wai-Ning Mei, Haekyung Jeong, Young Hee Lee, Jeong-O Lee, Duy Le and Zhengzheng Zhang.

References

[1] Collins P, Bradley K, Ishigami M and Zettl A 2000 *Science* **287** 1801–4

[2] Krüger M, Widmer I, Nussbaumer T, Buitelaar M and Schönenberger C 2003 *New J. Phys.* **5** 138

[3] Kong J, Franklin N R, Zhou C, Chapline M G, Peng S, Cho K and Dai H 2000 *Science* **287** 622–5

[4] Bolotin K I, Sikes K J, Jiang Z, Klima M, Fudenberg G, Hone J, Kim P and Stormer H L 2008 *Solid State Commun.* **146** 351–5

[5] Morozov S V, Novoselov K S, Katsnelson M I, Schedin F, Elias D C, Jaszczak J A and Geim A K 2008 *Phys. Rev. Lett.* **100** 16602

[6] Geim A K and MacDonald A H 2007 *Phys. Today* **60** 8 35

[7] Castro Neto A H, Guinea F, Peres N M R, Novoselov K S and Geim A K 2009 *Rev. Mod. Phys.* **81** 109

[8] Skomski R, Dowben P A, Driver M S, Kelber J A 2014 *Mat. Horiz.* at press

[9] Vázquez de Parga A, Calleja F, Borca B, Passeggi M, Hinarejos J J, Guinea F, Miranda R, Vazquez de Parga A L and Passeggi M C G Jr 2008 *Rev. Lett.* **100** 56807

[10] Zhou S Y, Gweon G H, Fedorov A V, First P N, De Heer W A, Lee D H, Guinea F, Castro Neto A H and Lanzara A 2007 *Nat. Mater.* **6** 770–5

[11] Leenaerts O, Partoens B and Peeters F M 2008 *Phys. Rev. B* **77** 125416

[12] Zhang Y H, Chen Y B, Zhou K G, Liu C H, Zeng J, Zhang H L and Peng Y 2009 *Nanotechnology* **20** 185504

[13] Wang X, Li X, Zhang L, Yoon Y, Weber P K, Wang H, Guo J and Dai H 2009 *Science* **324** 768–71

[14] Romero H E E H, Shen N, Joshi P, Gutierrez H R R, Tadigadapa S A A, Sofo J O O and Eklund P C C 2008 *ACS Nano* **2** 2037–44

[15] Romero H E, Joshi P, Gupta A K, Gutierrez H R, Cole M W, Tadigadapa S A and Eklund P C 2009 *Nanotechnology* **20** 245501

[16] Antonova I V, Mutilin S V, Seleznev V A, Soots R A, Volodin V A and Prinz V Y 2011 *Nanotechnology* **22** 285502

[17] Sato Y, Takai K and Enoki T 2011 *Nano Lett.* **11** 3468–75

[18] Liu L, Ryu S, Tomasik M R R, Stolyarova E, Jung N, Hybertsen M S S, Steigerwald M L L, Brus L E E and Flynn G W W 2008 *Nano Lett.* **8** 1965–70

[19] Balog R *et al* 2010 *Nat. Mater.* **9** 315–9

[20] Chen J H, Jang C, Adam S, Fuhrer M S, Williams E D and Ishigami M 2008 *Nat. Phys.* **4** 377–81

[21] Pirkle A, Chan J, Venugopal A, Hinojos D, Magnuson C W, McDonnell S, Colombo L, Vogel E M, Ruoff R S and Wallace R M 2011 *Appl. Phys. Lett.* **99** 122103–8

[22] Shishir R S and Ferry D K 2009 *J. Phys.: Condens. Matter* **21** 232204

[23] Tongay S, Berke K, Lemaitre M, Nasrollahi Z, Tanner D B, Hebard A F and Appleton B R 2011 *Nanotechnology* **22** 425701

[24] Fallahazad B, Kim S, Colombo L and Tutuc E 2010 *Appl. Phys. Lett.* **97** 123103–5

[25] Sun Z, Yan Z, Yao J, Beitler E, Zhu Y and Tour J M 2010 *Nature* **468** 549–52

[26] Adam S and Das Sarma S 2008 *Solid State Commun.* **146** 356–60

[27] Geim A K 2009 *Science* **324** 1530–4

[28] Wallace P 1947 *Phys. Rev.* **71** 622

[29] Slonczewski J and Weiss P P 1958 *Phys. Rev.* **330**

[30] Schedin F, Geim A K, Morozov S V, Hill E W, Blake P, Katsnelson M I and Novoselov K S 2007 *Nat. Mater.* **6** 652–5

[31] Weak P 2009 http://en.wikipedia.org/wiki/File:GrapheneE2.png

[32] Geim A K and Novoselov K S 2007 *Nat. Mater.* **6** 183–91

[33] Geim A K 2009 *Science* **324** 1530–4

[34] Castro Neto A H and Novoselov K 2011 *Rep. Prog. Phys.* **74** 082501

[35] Novoselov K S 2011 *Angew. Chem. Int. Edn.* **50** 6986–7002

[36] Castro Neto A H *et al* 2009 *Rev. Mod. Phys.* **81** 109–62

[37] Das Sarma S *et al* 2011 *Rev. Mod. Phys.* **83** 407–70

[38] Young A F and Kim P 2011 *Annu. Rev. Condens. Matter Phys.* **2** 101–20

[39] Avouris P 2010 *Nano Lett.* **10** 4285–94

[40] Compton O C and Nguyen S T 2010 *Small* **6** 711–23

[41] Sun Y, Wu Q and Shi G 2011 *Energy Environ. Sci.* **4** 1113–32

[42] Pumera M 2011 *Energy Environ. Sci.* **4** 668–74

[43] Brownson D A C, Kampouris D K and Banks C E 2011 *J. Power Sources* **196** 4873–85

[44] Balandin A A 2011 *Nat. Mater.* **10** 569–81

[45] Ratinac K R *et al* 2010 *Environ. Sci. Technol.* **44** 1167–76

[46] Pumera M 2011 *Mater. Today* **14** 308–15

[47] Lin Y M and Avouris P 2008 *Nano Lett.* **8** 2119–25

[48] Dan Y, Lu Y, Kybert N J, Luo Z and Johnson A T C 2009 *Nano Lett.* **9** 1472–5

[49] Zhou M, Lu Y H, Cai Y Q, Zhang C and Feng Y P 2011 *Nanotechnology* **22** 385502

[50] Yavari F, Kritzinger C, Gaire C, Song L, Gulapalli H, Borca-Tasciuc T, Ajayan P M and Koratkar N 2010 *Small* **6** 2535–8

[51] Moser J, Verdaguer A, Jiménez D, Barreiro A and Bachtold A 2008 *Appl. Phys. Lett.* **92** 123507

[52] Wehling T O, Novoselov K S, Morozov S V, Vdovin E E, Katsnelson M I, Geim A K and Lichtenstein A I 2008 *Nano Lett.* **8** 173–7

[53] Lu Y H, Chen W, Feng Y P and He P M 2009 *J. Phys. Chem. B* **113** 2–5

[54] Subrahmanyam K S, Kumar P, Maitra U, Govindaraj A, Hembram K P S S, Waghmare U V and Rao C N R 2011 *Proceedings of the National Academy of Sciences of the United States of America* **108** 2674–7

[55] Berashevich J and Chakraborty T 2009 *Phys. Rev. B* **80** 033404

[56] Krasheninnikov A V, Lehtinen P O, Foster A S, Pyykkö P and Nieminen R M 2009 *Phys. Rev. Lett.* **102** 126807

[57] Lu Y H, Zhou M, Zhang C and Feng Y P 2009 *J. Phys. Chem. C* **113** 20156–60

[58] Li Y, Zhou Z, Yu G, Chen W and Chen Z 2010 *J. Phys. Chem. C* **114** 6250–4

[59] Bekyarova E, Sarkar S, Niyogi S, Itkis M E and Haddon R C 2012 *J. Phys. D: Appl. Phys.* **45** 154009

[60] Sofo J O, Chaudhari A S and Barber G D 2007 *Phys. Rev. B* **75** 153401

[61] Ritschel M, Uhlemann M, Gutfleisch O, Leonhardt A, Graff A, Täschner C and Fink J 2002 *Appl. Phys. Lett.* **80** 2985

[62] Wang Y, Li A, Wang K, Guan C, Deng W, Li C and Wang X 2010 *J. Mater. Chem.* **20** 6490

[63] Gundiah G, Govindaraj A, Rajalakshmi N, Dhathathreyan K S and Rao C N R 2003 *J. Mater. Chem.* **13** 209–13

[64] Boukhvalov D W and Katsnelson M I 2009 *J. Phys.: Condens. Matter* **21** 344205

[65] Rafiee J, Mi X, Gullapalli H, Thomas A V, Yavari F, Shi Y, Ajayan P M and Koratkar N A 2012 *Nat. Mater.* **11** 217–22

[66] Wang W L and Kaxiras E 2010 *New J. Phys.* **12** 125012

[67] Bunch J S, Verbridge S S, Alden J S, Van der Zande A M, Parpia J M, Craighead H G and McEuen P L 2008 *Nano Lett.* **8** 2458–62

[68] Huang B, Li Z, Liu Z, Zhou G, Hao S, Wu J, Gu B-L and Duan W 2008 *J. Phys. Chem. C* **112** 13442–6

[69] Andzelm J, Govind N and Maiti A 2006 *Chem. Phys. Lett.* **421** 58–62

[70] Coletti C, Riedl C, Lee D S, Krauss B, Patthey L, Von Klitzing K, Smet J H and Starke U 2010 *Phys. Rev.* B **81** 235401

[71] Dong X, Fu D, Fang W, Shi Y, Chen P and Li L J J 2009 *Small* **5** 1422–6

[72] Bermudez V M and Robinson J T 2011 *Langmuir* **27** 11026–36

[73] Farmer D B, Golizadeh-Mojarad R, Perebeinos V, Lin Y-M, Tulevski G S, Tsang J C and Avouris P 2009 *Nano Lett.* **9** 388–92

[74] Rochefort A and Wuest J D 2009 *Langmuir* **25** 210–5

[75] Bekyarova E, Itkis M E E, Ramesh P, Berger C, Sprinkle M, De Heer W A A and Haddon R C C 2009 *J. Am. Chem. Soc.* **131** 1336–7

[76] An X, Simmons T, Shah R, Wolfe C, Lewis K M, Washington M, Nayak S K, Talapatra S and Kar S 2010 *Nano Lett.* **10** 4295–301

[77] Stankovich S, Piner R D, Nguyen S T and Ruoff R S 2006 *Carbon* **44** 3342–7

[78] Lu C H, Yang H H, Zhu C L, Chen X and Chen G N 2009 *Angew. Chem. Int. Edn.* **48** 4785–7

[79] Zhang Y H, Zhou K G, Xie K F, Zeng J, Zhang H L and Peng Y 2010 *Nanotechnology* **21** 65201

[80] AlZahrani A Z 2010 *Appl. Surf. Sci.* **257** 807–10

[81] Tournus F and Charlier J C 2005 *Phys. Rev.* B **71** 165421

[82] Wuest J D and Rochefort A 2010 *Chem. Commun.* **46** 2923–5

[83] Chakarova-Käck S D, Schröder E, Lundqvist B I and Langreth D C 2006 *Phys. Rev. Lett.* **96** 146107

[84] Krasnenko V, Kikas J and Brik M G 2012 *Physica* B **407** 4557–61

[85] Krepel D, Hod O 2013 *J. Phys. Chem.* C **117** 19477–88

[86] Huang P, Zhu H, Jing L, Zhao Y and Gao X 2011 *ACS Nano* **5** 7945–9

[87] Sarkar S, Bekyarova E and Haddon R C 2012 *Mater. Today* **15** 276–85

[88] Koehler F M, Luechinger N A, Ziegler D, Athanassiou E K, Grass R N, Rossi A, Hierold C, Stemmer A and Stark W J 2009 *Angew. Chem.* **48** 224–7

[89] Niyogi S, Bekyarova E, Itkis M E, Zhang H, Shepperd K, Hicks J, Sprinkle M, Berger C, Lau C N, deHeer W A, Conrad E H and Haddon R C 2010 *Nano Lett.* **10** 4061–6

[90] Paulus G L C, Wang Q H and Strano M S 2013 *Acc. Chem. Res.* **46** 160–70

[91] Park J and Yan M 2013 *Acc. Chem. Res.* **46** 181–9

[92] Bekyarova E, Sarkar S, Wang F, Itkis M E, Kalinina I, Tian X and Haddon R C 2013 *Acc. Chem. Res.* **46** 65–76

[93] Sarkar S, Bekyarova E and Haddon R C 2012 *Angew. Chem.* **51** 4901–4

[94] Sarkar S, Bekyarova E and Haddon R C 2012 *Acc. Chem. Res.* **45** 673–82

[95] Sarkar S, Bekyarova E, Niyogi S and Haddon R C 2011 *J. Am. Chem. Soc.* **133** 3324–7

[96] Pinto H, Jones R, Goss J P and Briddon P R 2009 *J. Phys.: Condens. Matter* **21** 402001

[97] Milián B, Pou-Amérigo R, Viruela R and Ortí E 2004 *Chem. Phys. Lett.* **391** 148–51

[98] Chen W, Chen S, Qi D C, Gao X Y and Wee A T S 2007 *J. Am. Chem. Soc.* **129** 10418–22

[99] Hsu C L, Lin C T, Huang J H, Chu C W, Wei K H and Li L J 2012 *ACS Nano* **6** 5031–9

[100] Abdurakhmanova N, Floris A, Tseng T C, Comisso A, Stepanow S, De Vita A and Kern K 2012 *Nat. Commun.* **3** 940

[101] Barja S, Garnica M, Hinarejos J J, De Parga A L V, Martín N and Miranda R 2010 *Chem. Commun.* **46** 8198–200

[102] Torrente I F, Franke K J and Pascual J I 2008 *Int. J. Mass Spectrom.* **277** 269–73

[103] Patterson T, Pankow J and Armstrong N R 1991 *Langmuir* **7** 3160–6

[104] Manna A K and Pati S K 2009 *Chem. Asian J.* **4** 855–60

[105] Chi M and Zhao Y P 2012 *Comp. Mater. Sci.* **56** 79–84

[106] Elias D C, Nair R R, Mohiuddin T M G, Morozov S V, Blake P, Halsall M P, Ferrari A C, Boukhvalov D W, Katsnelson M I and Geim A K 2009 *Science* **323** 610–3

[107] Otero R, Gallego J M, De Parga A L V, Martín N and Miranda R 2011 *Adv. Mater.* **23** 5148–76

[108] Qi Y, Mazur U and Hipps K W 2012 *RSC Adv.* **2** 10579

[109] Wang X, Xu J B, Xie W and Du J 2011 *J. Phys. Chem.* C **115** 7596–602

[110] Sun J T, Lu Y H, Chen W, Feng Y P and Wee A T S 2010 *Phys. Rev.* B **81** 155403

[111] Dong X *et al* 2009 *Phys. Rev. Lett.* **102** 135501

[112] Huang H, Chen S, Gao X, Chen W and Wee A T S 2009 *ACS Nano* **3** 3431–6

[113] Wang Q H and Hersam M C 2009 *Nat. Chem.* **1** 206–11

[114] Wang Q H H and Hersam M C C 2011 *Nano Lett.* **11** 589–93

[115] Tian X Q, Xu J B and Wang X M 2010 *J. Phys. Chem.* C **114** 20917–24

[116] Temirov R, Soubatch S, Luican A and Tautz F S 2006 *Nature* **444** 350–3

[117] Gustafsson J, Zhang H, Moons E and Johansson L 2007 *Phys. Rev.* B **75** 155413

[118] Johari P and Shenoy V V B 2011 *ACS Nano* **5** 7640–7

[119] Roos M, Künzel D, Uhl B, Huang H-H, Brandao Alves O, Hoster H E, Gross A and Behm R J 2011 *J. Am. Chem. Soc.* **133** 9208–11

[120] Kong L, Perez Medina G J, Colón Santana J A, Wong F, Bonilla M, Colón Amill D A, Rosa L G, Routaboul L, Braunstein P and Doudin B 2012 *Carbon* **50** 1981–6

[121] Xiao J *et al* 2010 *Phys. Chem. Chem. Phys.* **12** 10329–40

[122] Ortega J E, Himpsel F J, Li D Q and Dowben P A 1994 *Solid State Commun.* **91** 807–11

[123] Dowben P A 2000 *Surf. Sci. Rep.* **40** 151–247

[124] Garcia-Lastra J M, Rostgaard C, Rubio A and Thygesen K S 2009 *Phys. Rev.* B **80** 245427

[125] Zhang Z, Gonzalez R, Diaz G, Rosa L G, Ketsman I, Zhang X, Sharma P, Gruverman A and Dowben P A 2011 *J. Phys. Chem.* C **115** 13041–6

[126] Fang Y, Phuong N, Ivasenko O, Aviles M P, Kebede E, Askari M S, Ottenwaelder X, Ziener U, Siri O and Cuccia L A 2011 *Chem. Commun.* **47** 11255–7

[127] Jeong H K, Jin M H, So K P, Lim S C and Lee Y H 2009 *J. Phys. D: Appl. Phys.* **42** 065418

[128] Quintana M, Montellano A, Del Rio Castillo A E, Van Tendeloo G, Bittencourt C and Prato M 2011 *Chem. Commun.* **47** 9330–2

[129] Sharma R, Baik J H, Perera C J and Strano M S 2010 *Nano Lett.* **10** 398–405

[130] Shin H J *et al* 2010 *J. Am. Chem. Soc.* **132** 15603–9

[131] Candini A, Klyatskaya S, Ruben M, Wernsdorfer W and Affronte M 2011 *Nano Lett.* **11** 2634–9

[132] O'Mahony S, O'Dwyer C, Nijhuis C A, Greer J C, Quinn A J and Thompson D 2013 *Langmuir* **29** 7271

[133] Mao X *et al* 2013 *J. Am. Chem. Soc.* **135** 2181–7

[134] Akdim B, Pachter R, Kim S S, Naik R R, Walsh T R, Trohalaki S, Hong G, Kuang Z, and Farmer B L 2013 *ACS Appl. Mater. Interfaces* **5** 7470

[135] Katoch J, Kim S N, Kuang Z, Farmer B L, Naik R R, Tatulian S A and Ishigami M 2012 *Nano Lett.* **12** 2342

[136] Kim S N, Kuang Z, Slocik J M, Jones S E, Cui Y, Farmer B L, McAlpine M C and Naik R R 2011 *J. Am. Chem. Soc.* **133** 14480

[137] Ou L, Luo Y and Wei G 2011 *J. Phys. Chem.* B **115** 9813

[138] Alava T, Mann J A, Théodore C, Benitez J J, Dichtel W R, Parpia J M and Craighead H G 2013 *Anal. Chem.* **85** 2754–9

[139] Min S K, Cho Y, Mason D R, Lee J Y and Kim K S 2011 *J. Phys. Chem.* C **115** 16247

[140] Min S K, Kim W Y, Cho Y and Kim K S 2011 *Nat. Nanotechnol.* **6** 162

[141] Gowtham S, Scheicher R H, Ahuja R, Pandey R and Karna S P 2007 *Phys. Rev.* B **76** 033401

[142] Antony J and Grimme S 2008 *Phys. Chem. Chem. Phys.* **10** 2722

[143] Berland K, Chakarova-Kack S D, Cooper V R, Langreth D C and Schroder E 2011 *J. Phys.-Condens. Matter* **23** 135001

[144] Dion M, Rydberg H, Schroder E, Langreth D C and Lundqvist B I 2004 *Phys. Rev. Lett.* **92** 246401

[145] Le D, Kara A, Schroder E, Hyldgaard P and Rahman T S 2012 *J. Phys.: Condens. Matter* **24** 424210

[146] Cho Y, Min S K, Yun J, Kim W Y, Tkatchenko A and Kim K S 2013 *J. Chem. Theory Comput.* **9** 2090

[147] Misquitta A J, Podeszwa R, Jeziorski B and Szalewicz K J 2005 *Chem. Phys.* **123** 214103

[148] Tkatchenko A, DiStasio R A, Car R and Scheffler M 2012 *Phys. Rev. Lett.* **108** 236402

[149] Grimme S, Antony J, Ehrlich S and Krieg H 2010 *J. Chem. Phys.* **132** 154104

[150] Klimeš J, Bowler D R and Michaelides A 2011 *Phys. Rev.* B **83** 195131

[151] Balandin A A, Ghosh S, Bao W, Calizo I, Teweldebrhan D, Miao F and Lau C N 2008 *Nano Lett.* **8** 902–7

[152] Service R F 2009 *Science* **324** 875–7

[153] Lee C, Wei X, Kysar J W and Hone J 2008 *Science* **321** 385–8

[154] Zhang B and Cui T 2011 *Appl. Phys. Lett.* **98** 073116

[155] Arsat R, Breedon M, Shafiei M, Spizziri P G, Gilje S, Kaner R B, Kalantar-zadeh K and Wlodarski W 2009 *Chem. Phys. Lett.* **467** 344–7

[156] Gong K, Yan Y, Zhang M, Su L, Xiong S and Mao L 2005 *Anal. Sci.* **21** 1383–93

[157] Ohno Y, Maehashi K, Yamashiro Y and Matsumoto K 2009 *Nano Lett.* **9** 3318–22

[158] Yavari F, Chen Z, Thomas A V, Ren W, Cheng H-M and Koratkar N 2011 *Sci. Rep.* **1** 166

[159] Lu G, Ocola L E and Chen J 2009 *Nanotechnology* **20** 445502

[160] Nomani M W K, Shishir R, Qazi M, Diwan D, Shields V B, Spencer M G, Tompa G S, Sbrockey N M and Koley G 2010 *Sensors Actuators B Chem.* **150** 301–7

[161] Ko G, Kim H Y, Ahn J, Park Y M, Lee K Y and Kim J 2010 *Curr. Appl. Phys.* **10** 1002–4

[162] Lu G, Ocola L E and Chen J 2009 *Appl. Phys. Lett.* **94** 083111

[163] Lu G, Yu K, Ocola L E and Chen J 2011 *Chem. Commun.* **47** 7761–3

[164] Chen C W, Hung S C, Yang M D, Yeh C W, Wu C H, Chi G C, Ren F and Pearton S J 2011 *Appl. Phys. Lett.* **99** 243502

[165] Chu B H, Lo C F, Nicolosi J, Chang C Y, Chen V, Strupinski W, Pearton S J and Ren F 2011 *Sensors Actuators B Chem.* **157** 500–3

[166] Shafiei M, Spizzirri P G, Arsat R, Yu J, Du Plessis J, Dubin S, Kaner R B, Kalantar-Zadeh K and Wlodarski W 2010 *J. Phys. Chem.* C **114** 13796–801

[167] Yoon H J, Jun D H, Yang J H, Zhou Z, Yang S S and Cheng M M-C 2011 *Sensors Actuators B Chem.* **157** 310–3

[168] Cuong T V *et al* 2010 *Mater. Lett.* **64** 2479–82

[169] Massera E, Ferrara V L A, Miglietta M, Polichetti T, Nasti I and Francia G D I 2011 *Chem. Today* **29** 39–41

[170] Li W *et al* 2011 *ACS Nano* **5** 6955–61

[171] Ao Z M, Yang J, Li S and Jiang Q 2008 *Chem. Phys. Lett.* **461** 276–9

[172] Dua V, Surwade S P, Ammu S, Agnihotra S R, Jain S, Roberts K E, Park S, Ruoff R S and Manohar S K 2010 *Angew. Chem.* **49** 2154–7

[173] Cheng Z, Li Q, Li Z, Zhou Q and Fang Y 2010 *Nano Lett.* **10** 1864–8

[174] Kang X, Wang J, Wu H, Aksay I A, Liu J and Lin Y 2009 *Biosens. Bioelectron.* **25** 901–5

[175] Pereira V M, Castro Neto A H and Peres N M R 2009 *Phys. Rev.* B **80** 045401

[176] Gui G, Li J and Zhong J 2008 *Phys. Rev.* B **78** 075435

[177] Naumov I I and Bratkovsky A M 2011 *Phys. Rev.* B **84** 245444

[178] Kumar P, Skomski R, Manchanda P, Kashyap A and Dowben P A 2014 *Curr. Appl. Phys.* **14** S136–9

[179] Son Y W, Cohen M L and Louie S G 2006 *Phys. Rev. Lett.* **97** 216803

[180] Barone V, Hod O and Scuseria G E 2006 *Nano Lett.* **6** 2748–54

[181] Prezzi D, Varsano D, Ruini A, Marini A and Molinari E 2008 *Phys. Rev.* B **77** 041404

[182] Yang L, Cohen M L and Louie S G 2007 *Nano Lett.* **7** 3112

[183] Yang L, Park C H, Son Y W, Cohen M L and Louie S G 2007 *Phys. Rev. Lett.* **99** 186801

[184] Han M, Özyilmaz B, Zhang Y and Kim P 2007 *Phys. Rev. Lett.* **98** 206805

[185] Li X, Wang X, Zhang L, Lee S and Dai H 2008 *Science* **319** 1229–32

[186] Linden S *et al* 2012 *Phys. Rev. Lett.* **108** 216801

[187] Vo T H, Shekhirev M, Kunkel D A, Morton M D, Berglund E, Kong L, Wilson P M, Dowben P A, Enders A and Sinitskii A 2014 *Nat. Commun.* **5** 3189

[188] Prezzi D, Varsano D, Ruini A and Molinari E 2011 *Phys. Rev.* B **84** 041401

[189] Sessi P, Guest J R, Bode M and Guisinger N P 2009 *Nano Lett.* **9** 4343

[190] McCann E 2006 *Phys. Rev.* B **74** 161403

[191] Min H K, Sahu B, Banerjee S K and MacDonald A H 2007 *Phys. Rev.* B **75** 155115

[192] Mak K, Lui C, Shan J and Heinz T 2009 *Phys. Rev. Lett.* **102** 256405

[193] Zhang Y B, Tang T T, Girit T T C, Hao Z, Martin M C, Zettl A, Crommie M F, Shen Y R and Wang F 2009 *Nature* **459** 820

[194] Crowther A C, Ghassaei A, Jung N and Brus L E 2012 *ACS Nano* **6** 1865–75

[195] Zhou S Y, Siegel D A, Fedorov A V and Lanzara A 2008 *Phys. Rev. Lett.* **101** 086402

[196] Jiang Q G 2013 *Phys. Chem. Chem. Phys.* **15** 10859

[197] Nourbakhsh A *et al* 2011 *J. Phys. Chem.* C **115** 16619–24

[198] Sutter P 2010 *J. Am. Chem. Soc.* **132** 8175–9

[199] Chen S and Cai W 2010 *New J. Phys.* **12** 125011

[200] Matis B R 2012 *ACS Nano* **6** 17–22

[201] Wu X and Zeng X C 2009 *Nano Lett.* **9** 250–6

[202] Sheka E F and Shaymardanova L Kh 2011 *J. Mater. Chem.* **21** 17128

[203] Liu X, Wen Y, Chen Z, Lin H, Chen R, Cho K and Shan B 2013 *AIP Adv.* **3** 052126

[204] Mohanty N and Berry V 2008 *Nano Lett.* **8** 4469–76

[205] Kong L *et al* 2013 *RSC Advances* 10956–61